Send for DRF

C & author

# TECHNIQUES FOR THE MEASUREMENT OF PRESSURE IN SIMULATED SPACE ENVIRONMENTS

By

Paul R. Yeager

Head, Environmental Measurements Section

Langley Research Center

National Aeronautics and Space Administration



Societe Francaise des Ingenieurs et Technicians du Vide

Revue Le Vide (Techniques et Applications)

December 2-5, 1969

Grenoble, France



L-3934

# TECHNIQUES FOR THE MEASUREMENT OF PRESSURE IN SIMULATED SPACE ENVIRONMENTS

By
Paul R. Yeager

## ABSTRACT

An overall view is presented of the research program in effect at the Langley Research Center, NASA, to provide means to measure the pressures in simulated space environments from $10^{-3}$ torr to less than $10^{-13}$ torr. Space simulators designed for instrument development are described, and details of the operating techniques of these systems are presented. Gage calibration systems and methods are briefly discussed. Recent developments in both total and partial pressure gages, including time response characteristics, ion source improvements, lower X-ray limits, and improved residual gas analyzers, are presented.

# TECHNIQUES FOR THE MEASUREMENT OF PRESSURE IN SIMULATED SPACE ENVIRONMENTS

By

Paul R. Yeager

## INTRODUCTION

For the past several years there has been a strong effort by the Environmental Measurements Section of the Langley Research Center to provide instrumentation to accurately measure the pressure and gas composition of the LRC space simulation facilities. These pressures range from $10^{-3}$ to less than $10^{-13}$ torr in both atmospheric gases, residual sorbed gases, and outgassing products of many and exotic materials.

In order to provide these measurement capabilities, efforts have been made both in-house and on contract to universities, industry, and other government agencies to provide total pressure measurements, partial pressure measurements, residual gas analysis (RGA), calibration capability, and developmental systems. This paper reviews the recent and current programs and reports the results that are currently available on the research efforts in space simulation measurement.

## MEASUREMENT TECHNIQUES

The work on measurement techniques is divided into two basic areas: (1) total pressure measurement, and (2) partial pressure measurement. The efforts on total pressure measurement are directed toward areas where the unknown components of the gas being measured are small, so that gas composition errors may be neglected; the requirements for measurement accuracy are not

high, so that the time and expense of a residual gas analysis is not justified; and special applications where for one reason or another, a total pressure measurement is required. Partial pressure measurements are made whenever possible as the preferred means of making the most accurate measurements, and are usually made with a mass spectrometer.

(1) Total Pressure Measurements:

The work on total pressure gages has been divided into three areas; (1) time response, (2) reduction of X-ray (residual current) limit, and (3) increased sensitivity of gages.

Time response work has been done to establish gage characteristics for measurements in pulsed plasma systems and in other areas where the pressure changes rapidly with time. An example of this is measurements of radio frequency interference caused by a rocket exhaust plume. Since the interference is a function of plume shape and size, and the plume changes with pressure rise, it is necessary that the pressure gage respond rapidly because the vacuum chamber pumping system cannot evacuate the chamber as fast as the rocket exhaust gases are generated.

The work done in response time measurement has primarily been done with nude Penning gages since their pressure range and rugged structure make them very adaptable to this type of experiment. This work is reported in detail by Smith and Melfi (ref. 1) and is briefly described below. The experiments were performed over the range of $10^{-3}$ to $10^{-6}$ torr with a gage of the type shown in figure 1. Construction of the gage is shown below.

| Electrode Material | |
|---|---|
| Anode | Molybdenum |
| Cathode | Copper |

Gage Geometry

| | |
|---|---|
| Cylindrical Anode | |
| Length | 0.64 cm |
| Diameter | 2.54 cm |
| Thickness | 0.152 cm |
| Circular Cathode | |
| Diameter | 3.81 cm |
| Spacing | 1.27 cm |
| Thickness | 0.076 cm |
| Magnetic Field | $8 \times 10^{-2}$ Tesla |
| Voltage | 1750 Volts |

The dimensions and operating characteristics given were found to be the most suitable from among a wide variety tested. The experimental gage is shown mounted in a vacuum system (fig. 2) and a diagram of this system is shown in figure 3. In a typical operation, the system was pumped down to its ultimate pressure, the low $10^{-8}$ torr range, and the test gas was bled back into the system to establish the starting pressure. A microvalve was then pulsed to give a sharp pressure rise in the system. The output of the gage was recorded on an oscilloscope with a typical record being shown in figure 4. Since there is a small but finite delay time in the valve operation and the pressure pulse reaching the gage, the gage must be at least as fast in response as the record shows. The overall time response of the gage is shown in figure 5. From the experiments the following conclusions were drawn:

1. From the design data, it is concluded that:

(a) The construction of a cold-cathode gage which can be effectively operated above $10^{-3}$ torr is doubtful.

(b) Data from cold-cathode gages are repeatable when the gages are properly constructed.

(c) Subjecting the gage to overpressure for a short duration causes no significant change in the gage characteristics.

(d) The use of a perforated shroud around the gage improves its stability at higher pressures.

2. From the operational data, use of this type of gage as a means to measure very rapid pressure changes leads to the following conclusions:

(a) Location of the gage and conductance of the system is an important factor in the calculation of pressure as a function of time.

(b) Gages to be used for response-time measurements should have a maximum conductance and should be placed directly in the region for which the measurements are desired.

(c) Since the total test system, including the process for raising the pressure, is capable of indicating a pressure change from $10^{-6}$ torr to $10^{-3}$ torr in less than 100 microseconds, the gage must respond in less than 100 microseconds.

(d) At lower pressures the response time of the electronics (readout system) is likely to be the limiting factor.

The work on the reduction of X-rays has been centered around development of the buried collector (Melfi) gage and improvement of the orbitron gage.

Our work on the buried collector gage was first reported by Melfi and Clay (ref. 2) and later by Melfi (ref. 3). This particular gage evolved through several designs to the configuration shown in figure 6 and schematically in figure 7. The elements of the gage consist of a thoriated iridium filament, a closed-end grid, a shield plate, a focusing cup, and an ion collector. A

buried ion collector, 0.127 mm in diameter, is placed so that the exposed end is flush with the shield plate to give maximum sensitivity. The shield plate, which is held at filament potential, serves the dual purpose of drawing the ions into the collector region and shielding the ion collector from X-rays. This gives a further reduction in X-ray limit beyond that obtained by removing that portion of the collector within the grid cage. The focusing cup is held at grid potential so that ions are repelled to the collector, thus enhancing the sensitivity. With a collector to filament potential difference of -300 volts, a nominal gage constant of 25 $torr^{-1}$ is attained. This gives a 0.1 amp/torr sensitivity for emission currents (4 mA) in the low milliampere range where space charge problems are minimized. The X-ray background pressure for this gage was calculated to be $8 \times 10^{-13}$ torr. Measured background currents are below the equivalent $N_2$ pressure of $2 \times 10^{-12}$ torr.

The experimental work on the gage was carried out on two separate vacuum systems in order to first, determine gage sensitivity, stability and optimum operating parameters and second, find the low range operating characteristics of the gage. The first system, a gage calibration system, described in detail later, utilizes 500-liter/second ion pumps in conjunction with titanium sublimation and liquid nitrogen cryopanels to produce an ultimate chamber pressure of less than $4 \times 10^{-11}$ torr. This system generates known pressures in the calibration chamber by utilizing a constant pressure gas flowmeter for generating and measuring a gas flow rate $Q$ into the calibration chamber while pumping the gas from the chamber through a known conductance orifice at a known speed $S$. The pressure in the calibration chamber is then calculated by the relation: $P = Q/S$. The assumption is made that this gas flow rate $Q$ is much larger than that of all other gas sources and that the speed $S$ at the orifice

is much smaller than the pump speed. The calibration range of this system extends from $1 \times 10^{-9}$ to $5 \times 10^{-4}$ torr, with a calculated maximum measurement uncertainty in the determination of the pressure of ±5.5 percent. The second system (ref. 4) utilizes a turbomolecular pump to rough the gage chamber and a titanium pump down to the high $10^{-9}$ torr range. The system is then baked at $400^{\circ}$ C for 24 hours. Hydrogen and helium are expected to be the residual gases in this range and can be effectively handled by the sublimation pump. After the bake, the turbopump is sealed off and the ultimate pressure in the $10^{-12}$ torr range is attained by $LN_2$ sublimation pumping. A nude Helmer gage (ref. 5) is incorporated into this system to measure its ultimate pressure. This gage, as reported, uses approximately 6 mA emission current to give a 0.1 ampere/torr sensitivity. The ions are electrostatically focused $90^{\circ}$ to their entrance in the collector region, thereby reducing the X-ray background problem since only reflected X-rays can reach the collector. A suppressor grid is then used to suppress the photoelectrons back to the collector giving a further reduction in this background. This gage has a reported X-ray background of $\approx 1.5 \times 10^{-15}$ amperes, and can be effectively used to measure pressure in the $10^{-11}$ torr range.

For the first experiments, the buried collector gage was placed on the calibration system and a known pressure was set with $N_2$ gas at $2 \times 10^{-9}$ torr. The grid to filament voltage was set at 150 V. (No investigation of the electron trajectory was made because of the similarity between this gage and a standard commercial UHV gage.) Figure 8 shows a plot of gage constant versus emission current in the 7 to 0.02 mA emission range for collector voltages of 400, 300, and 200 V. In the 400 V case some interaction with the electric field about the grid structure was noted and excess filament power was required

to obtain the higher emission currents. For 200 V case, the loss of sensitivity in the mA emission range was significant. It was, therefore, decided to choose the 300 V case and operate at an emission current (4 mA) which would give approximately a 0.1 ampere/torr sensitivity. All further data on this gage was then taken with the following operating parameters:

$$V_{gf} = 150 \text{ V}$$

$$V_{cf} = 300 \text{ V}$$

$$i^- = 4 \text{ mA}$$

The cup is connected internally to grid potential while the shield may be connected to filament potential in the operational mode and grid potential during outgassing. A number of calibrations were made in $N_2$ gas of ion current versus pressure using known pressures as set in the calibration system. The gage is linear in the pressure range of $10^{-6}$ to $10^{-9}$ torr within the measurement uncertainty of the calibration system. From this an average gage constant of 20 $\text{torr}^{-1}$ was calculated giving 0.08 amperes/torr sensitivity and this value was used for all further data.

The gage was then transferred to the second system and a series of tests were performed to determine low pressure operating conditions using a previously calibrated Helmer gage as the reference standard.

The ultimate pressure of the system, approximately $1 \times 10^{-12}$ torr, was attained with both gages operating. These gages were then checked for spurious noise. Both gages, with the emission off, have background currents below $2 \times 10^{-14}$ amperes. After thorough outgassing, a plot of ion current of the buried collector gage versus ion current of the bent beam Helmer gage was made by bleeding in $N_2$ gas (fig. 9). This curve shows a residual current limit for the buried collector gage of approximately $2.2 \times 10^{-13}$ amperes. If we

assume the bent beam Helmer gage remains linear below $10^{-9}$ torr and a buried collector gage constant of 20 $torr^{-1}$ with 4 mA emission, the nitrogen equivalent residual limit would be approximately $2.6 \times 10^{-12}$ torr. It is felt that outgassing from the filament and desorbed gases from the grid could contribute to this limit as well as the X-rays.

Further efforts on low X-ray limit gages has been centered around the orbitron gage. This work has been divided into two parts: (1) theoretical analysis to determine optimum orbitron configuration and operating parameters and (2) design of electronic systems and experiments with variations on the basic orbitron configuration. The theoretical analysis was made primarily by Brock (ref. 6) and includes a thorough and comprehensive computer program to analyze all possible variables and their effect on the operation of the gage. To adequately describe this work requires a paper in itself, so a brief summary must suffice here. In previous studies of the orbitron only the space charge free potential distribution was considered. While the results of these studies may correctly describe the electron trajectories for a very low electron density stored in the rotating electron cloud, the results are not applicable to practical orbitrons since existing experimental data indicate that the electron density in the space charge cloud is not negligible. The space charge free analysis yields little, if any, insight into the dynamics of the orbitron since all the questions of substance involve the space charge dependent potential distribution. Questions concerning, for example: electrode geometry for optimum charge storage in the rotating space charge cloud, launcher location for optimum charge storage, anode potential for optimum charge storage, self-consistent orbit injection parameters, mean orbiting life-time of the electrons, orbit stability criteria, dependence of mean kinetic energy on stored charge,

injection (emission) current necessary to maintain optimum charge storage, ionization rate, and the ion energy distribution, cannot be answered without knowledge of the space charge dependent potential distribution.

The above observations clearly indicate that the analysis of the orbitron should be self-consistent if it is to be applicable to real orbitrons. That is, the analysis must be self-consistent in the sense that the differential equations which describe the electron motion must contain a potential distribution which is in part a function of average electron distribution within the space charge cloud, and thus take proper account of the electron motion. This appears to be a formidable task, since the self-consistent set of differential equations describing the electron motion (Force Equations, Poisson Equation, and Continuity Equation) reduce to an essentially nonlinear integral equation of a type for which no general solution is known (except, perhaps, in a few special, restricted cases). However, a solution to the self-consistent set of equations is possible using iterative, numerical methods.

The development of a self-consistent solution for the electron motion, charge density distribution and charge dependent potential distribution in an orbitron is based on the assumptions given below.

ASSUMPTIONS

1. The space charge is completely electronic.
2. The charge density distribution is sufficiently uniform in the Z-direction that its variation with Z may be neglected.
3. The charge density distribution is independent of $\theta$.
4. The time dependent component of the charge density corresponding to the collision loss rate and the balancing injection rate is negligible compared to the circulating current associated with the equilibrium charge density.

5. Allowed trajections are members only of the orbit subset which satisfies the stability criteria; excluding however, those members of this subset which are low order closed trajectories.

These assumptions are shown to be valid for practicable configurations and modes of operation.

Poisson's Equation must be solved for an arbitrary charge density distribution extending over an arbitrary region of the interelectrode space. It is therefore necessary to divide the interelectrode space into three concentric regions and solve the Poisson Equation in each. The solution for each region is then matched at its boundaries with the solutions for the adjacent regions. In the process, electrode boundary conditions are applied.

The charge density distribution as a function of the radial component of the electron velocity is derived from statistical reasoning. Although the same result may be derived by application of the continuity equation the statistical method directly yields a normalized charge distribution function such that the integral over the entire interelectrode space is equal to the total charge stored in the rotating electron cloud.

The differential equations (force equations) for the motion of an electron are solved for an arbitrary potential distribution. Only a solution for the velocity is required since the turning points may be obtained directly from the velocity equation, and a detailed knowledge of the orbit shape is unnecessary in nearly all meaningful questions. However, much can be inferred concerning the general orbit shape from various analytical results.

Bound electron trajectories having an arbitrary shape (eccentricity) are analyzed for stability. A stability criterion is developed which separates all possible trajectories into two subsets, stable and unstable. A new, free para-

meter is introduced which quantitatively specifies the stability of electron trajectories. It is found that the dynamic response to an arbitrary perturbation of the electron trajectories has a limit for stable trajectories but diverges without limit for unstable trajectories. It is also found that within the stable trajectory subset there exists a discrete series of closed, stationary trajectories. These trajectories may be eliminated by disallowing certain discrete values of the stability parameter.

At this point three equations have been obtained in terms of three unknown functions: the potential distribution, the charge density distribution, and the radial component of the electron velocity. The imposition of the stability constraint which assures that the rotating electron cloud is populated with electrons having long probable lifetimes, completes the specification of the system. Solving this system of equations for the potential distribution yields a nonlinear integral equation for which a particular solution is possible using numerical techniques. By numerical integration and iteration, a solution having any prescribed accuracy may be obtained.

The radial component of the electron velocity corresponding to the space charge free potential distribution is taken as a first approximation to the radial velocity, for use in the charge density distribution equation. This first approximation to the charge density distribution is twice integrated, numerically, and the result used to obtain a first approximation to the space charge dependent potential distribution.

The numerical integrations require the specification of the limits of integration which in turn requires the specification of the ratio of turning point radii. Restricting further consideration to optimized total charge configurations only reduces the number of system parameters from 6 to 5 and

allows the retention of some generality in the sense that instead of finally obtaining a single particular solution for a specific set of parameters, a subset of particular solutions is obtained. It is found that optimization of the total charge stored in the electron cloud corresponds to locating the inner boundary of the cloud very near the anode surface. Incorporating this result provides a method of assuring that the ratio of turning point radii do not change in subsequent integrations.

The following are the prescribed parameters and derived parameters in the order of progress.

| PRESCRIBED PARAMETERS | DERIVED PARAMETERS |
|---|---|
| $r_i \simeq R_i$ | $\frac{r_o}{r_i} = 2.59$ |
| $\alpha_o^2 = \frac{1}{3}$ | $\alpha_\beta^2 = 0.684$ |
| $\beta = 1$ | $N_L = \frac{4\pi\varepsilon_o \beta T(r_o)}{\alpha_\beta^2 e^2 \left[ \mathrm{Ln} \frac{r_o}{r_i} - g_1 (\alpha_o, 1) \right.}$ |
| $T(r_o) = 50$ eV | $N_L = 0.825 \times 10^9$ cm $^{-1}$ |
| $H = -T(r_o)$ | $\frac{R_o}{R_i} = 5.13$ |
| | $V = 385$ VOLTS |
| | $V_{b_1} = 100$ VOLTS |

$\left\langle \frac{r}{r_o} \right\rangle = 0.746$

$\langle v \rangle = 6.45 \times 10^{8} \frac{cm}{sec}$

$\langle T \rangle = 119$ eV

$(\dot{N}_{Ar^+})_L = 6.6 \times 10^{18} \, P_T \left( \frac{Ar^+}{sec} \right)_L$

$(i_{Ar^+})_L = 1.06 \, P_T (amp)_L$

---

$R_o = 2.5$ cm

$r_o = 1.26$ cm

$r_i = 0.49$ cm

---

$L = 10$ cm

$(P_T)_{max} < 6.6 \times 10^{-5}$ Torr

$R_L = 0.05$ cm

$i_e = 0.645$ ma

$L' = 0.5$ cm

$\frac{i_e}{i_\theta} = 4.47 \times 10^{-3}$

$\frac{\dot{N}_{Ar^+}}{N_e P_T} = 1.63 \times 10^{-4}$ Torr$^{-1}$

$\frac{S_{Ar^+}}{C_\perp} = 2$ Liters/sec

$\langle \tau_{Ar^+} \rangle = 8.4 \times 10^{-7}$ sec

$(N_{Ar^+})_L = 5.5 \times 10^{12} \, P_T (A_r^+)_L$

The following conclusions may be drawn from the results developed in the preceding orbitron analysis:

(1) The space charge dependent potential distribution, for maximum charge stored stably in the rotating electron cloud, is substantially lower than the space charge free potential distribution. This confirms the suspicion that a space charge free analysis has limited utility.

(2) The maximum charge that may be stored stably in the rotating electron cloud is about the same as may be stored on one plate of a cylindrical capacitor of the same dimensions at the same anode potential.

(3) The maximum charge stored stably is approximately a linear function of anode potential (other parameters fixed). The ion production rate (per unit length of electron cloud) increases slower than the anode potential (other parameters fixed).

(4) Maximizing the charge stored stably requires that the electron trajectory inner turning point be very near the anode surface.

(5) The charge stored stably increases with increasing anode radius and decreasing outer cylinder radius (however for all other parameters fixed, the outer cylinder radius cannot be less than a certain lower limit).

(6) The feedback mechanism, which regulates the total population of the electron cloud at its maximum value consistent with stability requirements, is operative only for an inner turning point location very near the anode surface. For all larger inner turning point locations the cloud population must be regulated by other (external) mechanisms. The possibility of over populating the electron cloud presents a grave hazard if the inner turning point is not near the anode surface.

(7) Orbit insertion parameters must be accurately controlled to achieve optimum charge storage. Deviation in orbit insertion parameters results in unstable trajectories, short orbiting life times, and low ion production rate.

(8) For many configurations or modes of operation, the ratio of emission current to ion current increases with increasing anode potential.

(9) Ion gage sensitivities of the order of $10^4$ and $10^5$ $torr^{-1}$ can be achieved for conventional size devices.

(10) Several modes of operation are possible, for orbitron ion gages, which are substantially free of residual current.

Relatively high ionic pumping speeds are attainable in orbitron ion pumps. For example: an orbitron pump about the size of the magnetron gage (Redhead) and operated at the same anode potential would have an Argon speed of about 2 liters/sec. Similarly, a 5 cm diameter, 20 cm length orbitron pump operated at 10KV would have an Argon speed of about 65 liter/sec.

(11) The computational task associated with obtaining a precise solution to the orbitron problem appears to be less formidable than was suspected at first, since the comparison implies that the iteration process converges rapidly.

Other work on the orbitron gage has been concerned with actual experiments with various configurations of the orbitron at low pressures. The use of shield guards to act as ion reflectors to increase sensitivity is being studied along with filament position and electron injection parameters. The results are not yet available from these experiments.

In addition to general engineering work to improve gage sensitivity, of special interest has been the work carried out for us by Schwarz on the quadrupole ionization gage (ref. 7). The main points in developing a gage of

this type are:

1. Low x-ray limit, which implies that electron density decreases with pressure, or that few high energy electrons strike solid surfaces.

2. Elimination of the magnetic field.

3. Electron path length as long as possible.

These points were achieved by the use of a double quadrupole system which resembles a Penning type ion gage. The main difference is that instead of using a magnetic field for keeping the electrons in the center of the tube, use is made of quadrupole optics. The quadrupole system uses a radio frequency oscillator tuned so that only electrons are moving on stable trajectories within the center of the tube. A dc potential is superimposed on the radio frequency and also applied to a ring-shaped midpoint electrode. At the other end of the tube, the electrons encounter an inverse field due to a disc electrode which is at the same potential as the cathode. The electrons will thus remain in the tube until they hit gas atoms or molecules. Some of the ions are collected at a screen surrounding the entire electrode structure. The standard solutions to the quadrupole equation were used to determine the operating parameters for the gage. In this gage a frequency of 200 MHz was used which determines the ratio of the peak voltage $U_o$ and the superimposed dc voltage $U_{dc}$. For electron focusing the ratio $U_o/U_{dc}$ equals 6.05. This means that for a peak voltage $U_o$ = 165 volts, the dc potential should be $U_{dc}$ = 27 volts. The gage has always been tuned for maximum collector current which coincided with the theoretical relationship for best electron focusing. Under ideal conditions the unperturbed electrons will move indefinitely back and forth along the trajectories. The number of unperturbed electrons will increase as the pressure decreases. At pressures of $10^{-13}$ torr an electron will have a mean free

path of $10^{10}$ cm. An electron of such a mean free path will travel back and forth in the tube as long as "8 minutes" until it suffers a collision, which could lead to ionization. Assuming a 10% probability for such an event at a pressure of $10^{-13}$ torr, an ion current of the order of microamperes can be expected, and such ion currents have been reached in experiments.

Figure 10 shows a schematic drawing of the gage. The screen Sc collects the ions which were measured by a sensitive electrometer. The optimum negative potential was $U_s = -77$ volts against the cathode. The disc Co was connected with the cathode C. The cathode was a hairpin filament heated by a dc power supply. The ring AR was connected with the four rods R and had a potential of $U_{dc} = +27$ volts. A simple milliamperemeter A was inserted to measure the initial electron emission $i^-$. The radio frequency was fed into the rods by using the rods themselves as transmission lines. The peak voltage was obtained by inserting an impedance between two pairs of opposite rods. The total length of the electrode structure was 10 cm, and the internal radius as defined above was $r_o = 1$ cm.

Calibration curves were made at different RF power inputs and different electron emission currents. By adjusting the power supply for heating the filament, the emission current was set with only the dc potentials on. After feeding in the RF frequency with the correct peak potential, the emission current, as measured at the milliamperemeter A, dropped down to 1 to 10% of its initial value. This means that due to electron focusing and oscillations a negative space charge had built up and prevented further electron emission of the cathode.

The fact that the emission current dropped to such a low value means also that very few electrons of high energy really hit solid parts in the tube.

Figure 11 shows a calibration at an initial electron emission of 100 microamperes and an RF power transmitted into the quadrupole gage of about 20 watts.

The above briefly hits at the main points of total pressure measurement research being carried out or supported by the Langley Research Center of NASA. However, a large portion of the research is centered around partial pressure measurements, and this work is described in the next section.

(2) Partial Pressure Measurements

Work in partial pressure measurements has been limited almost exclusively to the mass spectrometer. Not only are residual background measurements made in this way, but in instances where accuracy of measurement is required and there is some question of test gas purity, the mass spectrometer, in one of its forms, is used as the measuring instrument.

In beginning development of improved mass spectrometers, the spectrometer was divided into three subsystems; (1) the ion source, (2) the mass separator, and (3) the ion detector. Our surveys of the state of development of the three areas indicated that the mass separator section, as represented by sectors, time-of-flight, and quadrupoles, was receiving adequate attention from other researchers and was the best developed of the three areas. We therefore concentrated on the development of ion sources as a primary area, and ion detectors as a secondary area. Backup work of a general nature has also been done on complete systems at very low pressures to establish system operating parameters and to determine optimum conditions for accurate measurement of residual gases.

The principle work in ion sources has been the development of a cold-cathode magnetron ion source (CCIS) for use with quadrupole mass spectrometers.

The details of this work are reported by Torney, et al, (ref. 8) and will be briefly reviewed here.

This program began with a two fold purpose: (1) to develop an ion source that had a higher ion production rate than conventional hot filament sources, and (2) to develop a source that would not react with gases as hot filaments do and thus produce a cleaner more representative sample of the gas to be measured. Both of these goals have been met. The basic design of the source is shown schematically in figure 12. This design was chosen after a number of configurations of the cold-cathode ion source (CCIS) were considered for possible application. These sources all involved a magnetically confined electrical discharge in a low pressure gas. Radioactive and other cold discharges were also considered but rejected primarily for sensitivity reasons. Of the numerous types of cold-cathode discharge devices, the magnetron type discharge (after Redhead) was selected, primarily because of its high sensitivity. An ion source was designed and built using the Redhead magnetron structure, but with a small remnant stub replacing the normal cathode spool construction. The preliminary source was designed to study the properties of ion beams extracted from the source. To this end, retarding field techniques were used in conjunction with a simple Faraday cup ion collector to measure the emergent beam. After preliminary investigation of various extraction methods, studies were made of the energy spread of the ion beam. A relatively large flux of low energy ions was noted under optimum conditions. This flux of ions was measured after passing through an aperture of 3 mm. The resultant ion source sensitivity was approximately 5 mA/torr (nitrogen). The total energy spread of 96.8% of the ions was between 0 and 31.5 eV. This figure is within the acceptable limits for axial energy spread for a small quadrupole analyzer.

It became obvious from early investigations of the ion source that the only analyzer capable of dealing with the relatively large CCIS energy spread was a quadrupole. It was not obvious which of the number of quadrupole operating modes would be most favorable for the CCIS, or if, indeed, any modes were. A careful analysis was, therefore, made of the quadrupole theory to define the optimum conditions. The results of this study showed that one mode is preferable to the others. Summarized briefly, it was shown that the so-called "constant peak width" ($\Delta m$ = constant) mode is preferable for the following reasons:

(a) Peak width is nearly independent of mass.

(b) Mass scale is linear throughout the mass range.

(c) Maximum allowable transverse ion energy (for 100 percent transmission) is independent of mass.

(d) Maximum allowable axial ion energy is also independent of mass.

(e) For 100 percent transmission, the selected mode will permit a larger beam diameter (higher sensitivity) than other modes.

(f) Requirements of frequency and voltage stability are less stringent for the chosen mode, particularly at lower masses.

Having demonstrated that a cold-cathode ion source will produce a beam of ions acceptable to a quadrupole analyzer, further work was begun in improving the source design to its fullest extent. The improved source contained a probe for measuring ion energy distribution through a very small (1 mm) simulated quadrupole entrance aperture. The probe's position was adjustable relative to the ion exit aperture. The design included an electrostatic lens and provision for comparing sensitivities with and without the lens. Also included was a provision for defining optimum ion extraction conditions. Modifications were also made in the magnetic field geometry used in the feasibility study.

Cylindrical ceramic magnets were used to reduce external bulk. Elimination of internal pole pieces improved beam geometry at the ion exit aperture and generally reduced internal sources of outgassing.

Methods of optimizing sensitivity without the lens were studied first. The sensitivity and ion energy distribution were examined (using retarding potential methods) as a function of extraction conditions. It was discovered that a large electron component was present in the beam and that certain abnormally large sensitivities observed were connected with the electron beam component. Subsequent data was, therefore, examined critically for possible misconceptions of this nature.

The highest sensitivity obtained with optimum ion extraction conditions and for an energy distribution acceptable to a quadrupole (0-30 eV) was 5.5 mA/torr (nitrogen). This value was measured at two nodes along the axis of the exiting beam. This sensitivity, obtained through the 1 mm diameter probe aperture compares very favorably with a somewhat lower figure obtained with a 3 mm diameter aperture used in the earlier study. A minimum sensitivity improvement of one decade was achieved without the use of a lens.

Improvements in sensitivity through the use of an electrostatic lens were also investigated. However, it was finally concluded that the lens offered no advantages and the use of the lens was discontinued.

Once the improved model of the ion source was completed, it was mated to a commercial quadrupole for evaluation. Pertinent specifications from the theoretical standpoint are as follows: Operating frequencies ($\nu$) are 5.3 mHz and 3.3 mHz on the low and medium mass ranges, respectively. Maximum available rod potential (V) is 1000 volts. The radius ($r_o$) of the circle inscribed

by the quadrupole rods is 2.7 mm. The entrance aperture diameter is also 2.7 mm. Rod lengths are 11.3 cm.

The final design of the cold-cathode ion source (CCIS) is a modification of the Redhead magnetron gage. To allow ion extraction, the single spool shaped cathode design used in the gage is separated into two cathodes, one with a remnant stub ($K_1$) which is 9.7 mm long and 3.1 mm in diameter. All remaining electrode dimensions remain as in the Redhead gage. The horseshoe magnet ordinarily used has been replaced by hollow cylindrical ceramic magnets. Dimensions and field strengths of the magnets used are given later.

Source electrodes are supported on a stainless steel cylindrical housing maintained at ground potential. Auxiliary cathodes are welded to it directly. The anode is attached and insulated by sapphire spheres. It is not perforated as in the Redhead gage. Cathodes $K_1$, and $K_2$ are supported and insulated by glass studs. This arrangement provides independent electronic access to the anode and each cathode; it likewise provides a guard ring design which, by preventing leakage between electrodes prevents interference with low level current detection.

The source housing is perforated and attached to the quadrupole with heavy refractory wire and a slotted sleeve; distance between the faces of $K_2$ and the quadrupole aperture plate was maintained at 2.4 mm (as close as possible without causing arcing between electrodes).

Tungsten mesh screens were used over the $K_2$ aperture and the quadrupole entrance aperture for the following reasons: (a) to allow testing of the effect of potential differences between these components without causing beam defocusing, (b) to isolate magnetron and quadrupole electric fields and, (c) to flatten the magnetron potential distribution at $K_2$ which otherwise

bulges through the $K_2$ aperture; this is to reduce ion defocusing and resultant sensitivity losses.

The CCIS/Quadrupole performance was investigated as a function of the parameters discussed below, first to determine optimum source operating conditions and second, to note the resultant spectrometer response to mass and pressure variations. During the first part of the investigation, nitrogen was used as the test gas at a pressure of $5.4 \times 10^{-9}$ torr. Initially, a 5.0 kV anode potential was used and cathode potentials $V_{K1}$ and $V_{K2}$ were kept at zero volts; thereafter, values were used which successively were shown to give the best resultion and sensitivity.

Performance vs. quadrupole resolution setting.-A family of nitrogen spectra were recorded as a function of quadrupole resolution dial settings. The latter correspond to ratios of dc and rf rod potentials, U and V respectively, in Paul's equation for quadrupole spectrometer resolution:

$$\frac{M}{\Delta M} = \frac{0.126}{0.16784 - U/V}$$

where M is the atomic mass and $\Delta M$ the peak width at its base. Spectral resolution changes were determined by comparing the full width at half maximum (FWHM) of the nitrogen peaks. Experimental resolution improved as dial settings proceeded toward higher theoretical resolution; sensitivity correspondingly decreased (as prediced by theory) until a setting was reached beyond which sensitivity continued to decrease with no further resolution improvement. This setting was then selected as optimum and used in subsequent experiments.

Performance vs. CCIS anode potential.-As with resolution setting experiments, FWHM measurements were made vs. anode potential ($V_A$) on a family

of nitrogen spectra. This was done both on the low and medium mass ranges (1-50 amu and 10-150 amu, respectively). The optimum value of $V_A$ for both ranges was in the vicinity of 2.0 kV (compared with 5.0 kV normally used in magnetron total pressures gages).

Performance vs. CCIS magnet position.-Using the optimum resolution setting and optimum anode discussed above, spectra were recorded against magnet position; first axially and then rotationally. Positions giving optimum resolution, as determined by FWHM, were selected. Unlike spectral variations with resolution setting and with anode potential, no sensitivity loss accompanied the positionally improved resolution. Resolution was found optimum when the magnet's center coincided with the midplane between cathodes $K_1$ and $K_2$. A ±3 mm axial magnet movement caused about a 20% broadening of the peak's FWHM. A 10% FWHM maximum variation occurred with rotational positioning.

Performance vs. CCIS ion retarding potential.- Acceleration and retardation of ions prior to their entrance to the quadrupole was effected by equal alteration of cathode potentials $V_{K1}$ and $V_{K2}$ while the quadrupole entrance aperture was maintained grounded. Acceleration was found to degrade quadrupole resolution while retardation improved it. This improvement, coupled with that obtained by lowering the anode potential, points to high ion energy as an important resolution limiting factor.

Nitrogen peak narrowing is produced by increasing retardation potentials. A 300 volt retardation potential was found optimum, when accompanying a 2.0 kV (later 2.2 kV) anode potential. For this determination the 10% valley criterion was used, the FWHM criterion being abandoned due to improved resolution.

Performance vs. potential between CCIS cathodes.-When making cathode potential $V_{K1} > V_{K2}$, resolution deteriorated obviously. For $V_{K1} < V_{K2}$, two conditions were tested: (1) with $V_{K2}$ at - 300 volts, resolution remained constant and sensitivity declined, (2) with $V_{K2}$ at zero volts, resolution improved but not to the extent achieved by equal variation of cathode potentials.

Performance vs. magnet size.-Experiments heretofore described, were performed with a hollow, cylindrical, ceramic magnet stack with an 11.4 cm o.d., 4.8 cm i.d., and a 5.7 cm length. Most of these experiments were repeated using a smaller magnet stack with an 8.9 cm o.d., 4.8 cm i.d., and 3.8 cm length. Axial magnetic flux densities, in gauss, for the large and small magnets, respectively, were as follows:

(1) on axis at the magnet's center, 1220 and 838.

(2) on axis at the magnet's edge, 397 and 368.

(3) on the inside wall of the magnet at the magnet's center, 1426 and 957.

The spectra obtained with the small magnet were very similar to those obtained with the large magnet. Resolution at this stage of investigation allowed peak separations of 3.0 amu and 1.5 amu (using the 10% valley criterion) on the medium and low mass ranges. This compares with 2.5 amu and 1.5 amu, respectively, for the large magnet. Sensitivity was slightly better than half that obtained with the large magnet. Most significantly, the small magnet displayed comparatively large operating mode instabilities; during one mode change, the entire nitrogen peak temporarily disappeared.

Further development might establish reliable operation with little or no loss of resolution or sensitivity, perhaps for still smaller magnets. At

present, however, the larger magnet gives a more stable and sensitive performance.

The experiments proved that the CCIS was indeed a suitable ion source for ultra high vacuum work. A comparison of the sensitivity of the CCIS versus the standard hot filament source for the same quadrupole is given below.

Sensitivity (ma/Torr)

| Gas | CCIS | | Hot Filament |
|---|---|---|---|
| | $3 \times 10^{-9}$ Torr | $1 \times 10^{-7}$ Torr | $1 \times 10^{-7}$ Torr |
| $He^4$ | .077[a](L) | 0.064 (L) | .042 (L) |
| $Ne^{20}$ | .130[a](L) | 0.100 (L) | .068 (L) |
| $N_2^{28}$ | .400 (L) | 0.820 (L) | .250 (L) |
| $A^{40}$ | .730 (L) | 1.200 (L) | .260 (L) |
| $A^{40}$ | .380 (M) | 0.780 (M) | .290 (M) |
| $Kr^{84}$ | .740 (M) | 1.200 (M) | .350 (M) |

a = (extrapolated)

It is seen that CCIS sensitivities exceed those of the hot-cathode source over the range of parameters investigated, even though the hot-cathode source was operated at relatively high emission current. The sensitivity advantage increases with atomic number; under low mass range operating conditions, the CCIS/hot-filament sensitivity ratio increases from 1.5 to 4.6 over the mass range 4 amu to 40 amu. Absolute sensitivities range from a low of .064 mA/torr for helium to a high of 1.2 mA/torr for krypton and argon. The maximum sensitivity variation with pressure for any particular gas is a factor of two over the approximately two decades investigated.

The sensitivity variation with mass is caused by variations both in the ion transmission of the quadrupole and in the ionization efficiency of the source. The quadrupole manufacturer supplied electronic means for adjusting relative mass sensitivities but these controls were not investigated.

A considerable amount of effort has been put into the development of counting techniques for very low density measurements. This effort has been in conjunction with the development of the CCIS. The work is described in detail by Torney, et al, (ref. 8) and consists primarily of finding the optimum means of increasing the signal to noise ratios of currents from electron multipliers under conditions of ultra high vacuum. The approach is to use pulse counting techniques so that the effects of gain change in high gain electron multipliers is largely eliminated in making measurements of molecular number density. Other refinements, such as offset multipliers to reduce photon generated noise have also been investigated. The general program is described below.

The primary aim of the investigation is to improve the reliability of low pressure measurements by improving the overall signal-to-noise (S/N) ratio of both total and partial pressure measuring devices. A high gain, low noise, electron multiplier is used in conjunction with appropriate ion counting circuitry to discriminate against the undesired noise. The cold-cathode ion source/quadrupole mass filter was employed as a partial and total pressure measuring device in these investigations. The electron multiplier is commercially available as standard equipment of the quadrupole analyzer. The output of the multiplier was readily adapted to a commercial pulse counting instrument (nuclear scaler).

The performance of the spectrometer has been investigated using both dc current and ion counting detectors for comparison and for other experimental purposes to be described later. The work program, which was largely experimental in character, has the following specific objectives:

(1) To evaluate the ion source-electron multiplier system, by measuring the ion current incident upon the cathode and the pulse arrival rate at the anode and to determine the ion accelerating voltage required to obtain a secondary electron yield of at least one.

(2) To investigate the feasibility of applying pulse height analysis techniques to discriminate between pulses produced by ions and those produced by photons or soft x-rays.

(3) To determine the maximum pressure that may be measured without saturating either the electron multiplier or pulse-counting circuit.

(4) To determine the operating characteristics of the ion source - mass filter - pulse counting system, both as total and partial pressure measuring devices.

(5) To study the performance of the system under extreme high vacuum conditions and to obtain calibration data to as low a pressure as possible.

Ion Counting Techniques - General Considerations

Advantages.-The basic partial pressure sensitivity of modest resolution ($\frac{M}{\Delta M} \leqq 100$) residual gas analyzers (RGA's) lies in the range of $5 \times 10^{-4}$ to $1 \times 10^{-5}$ amperes per torr for nitrogen (mass 28). Without the aid of an electron multiplier, such instruments are limited to an ultimate partial

pressure detectability in the realm of $2 \times 10^{-11}$ to $1 \times 10^{-9}$ torr, nitrogen, assuming that the minimum detectable ion current is $1 \times 10^{-14}$ amperes. The electron multiplier becomes an absolutely essential part of the dc analog ion detector, if improved sensitivity and S/N ratio of the instrument are required.

It is generally recognized that the stability of electron multipliers is inadequate to provide reproducible, quantitative data unless frequent gain measurements are made. Manufacturers of commercial RGA's report that a short-term reduction in multiplier gain of a factor of ten or more is typical initially and they recommend periodic gain measurements for greater reliability. Such instruments are now designed to provide a simple and expedient means of routinely measuring the gain. Special connections are provided for measuring the ion current at the first dynode and for measuring the electron current output of the multiplier. The gain is readily measured provided that the first dynode current is not below the detectability limits discussed above. If however, the RGA is operating at extremely low pressures, it is impossible to measure the gain of the multiplier and therefore, the sensitivity of the spectrometer cannot be measured directly.

Ion counting techniques offer a possible solution to this problem. All measurements are made at the output of the multiplier, thereby avoiding the difficulties of measuring very small currents at the input. The measurement involves simply the output counting rate (ions/second) and the output dc electron current. Assuming that the detector counts all ions striking the input of the multiplier, the input current is simply:

$$I_{in} = eR$$

where e = electron charge ($1.6 \times 10^{-19}$ coulombs) and R is the measured ion

counting rate in ions/sec. Appropriate correction must be made for multiply-charged species. For singly charged species, the gain for a particular mass becomes:

$$G_m = \frac{I_o}{R} \times 6.25 \times 10^{18}$$

where $I_o$ is the output electron current in amperes. This measurement includes the gain-dependancy of the multiplier on the ionic mass since $I_o$ will depend on mass.

Although ion counting techniques offer the important advantage of gain measurement at the output, a number of other advantages may also result therefrom.

Depending on certain noise factors largely determined by the spectrometer's ion source, it is possible to discriminate against a substantial portion of undesired noise by means of simple pulse height discrimination. The S/N ratio (compared to dc detectors) can be improved by a factor of 100 or more. The degree of improvement depends on the type of ion source-analyzer and on the detector design and on electron multiplier characteristics.

The present work indicates that with the very high gain/low noise multipliers recently made available, it is possible to circumvent nearly all gain instability in the multiplier (both short and long term). Thus the ion counting detector not only can reduce the uncertainties in detector gain, but shows promise of ultimately completely eliminating gain dependance.

In addition, the use of ion counting techniques eliminates the mass and charge dependancy of the multiplier since the detector response is related only to the number of events and not the m/e ratio of the ions and to their respective momenta. While this fact does not permit a direct one-to-one correlation between observed counting rate and partial pressure, it does

eliminate the detector as a contributor to the spectrometer's partial pressure response characteristics.

Finally, the use of counting techniques provides a direct output for digital data acquisition and analysis using computers, which have proven to be valuable in interpreting complex spectra and in analyzing large amounts of repetitive data.

Disadvantages.-The counting rate method of detecting ions involves the use of complex electronic equipment. For instance, a preamplifier, a non-overloading amplifier and an amplitude discriminator precede the counting equipment. Automatic mass scanning and data acquisition and recording equipment will obviously be more complex than the corresponding dc equipment. Of course, rate meter circuitry may be used to simplify the essential equipment with some sacrifice in accuracy. For routine qualitative analysis of UHV conditions, the increased complexity and expense of fully automated systems is not justifiable. For quantitative and reliable UHV measurements the relatively simple electronics used during this study may be employed very effectively.

Cold cathode ion source/quadrupole.-The CCIS/Quad was modified by the addition of a 14 stage focused dynode (Be-Cu) electron multiplier.

Electronics for ion counting.-Figure 13 is a block diagram of the equipment used during the ion-counting studies. In general, the equipment is a simple inter-connection of power supplies for operation of the CCIS, together with the quadrupole electronics console. A sweep voltage was derived from the quadrupole electronics to provide the x-axis (mass scale) on the X-Y recorder. An electrometer was employed to detect and record the ion currents at various mass peaks and to measure electron multiplier gain.

Counting data was taken with the simple configuration of standard nuclear scaling equipment shown. The linear pulse height discriminator included in the non-overloading pulse amplifier was used to obtain integral pulse height distribution data for signal and noise and to also discriminate against noise.

The counting equipment used has a relatively low frequency response of 100 kHz. With faster counting equipment the range of counting rates can easily be extended to the order of 10 mHz. The limitation of the present equipment together with other electronic considerations such as resolution loss etc., will be discussed shortly.

## Experimental Results

Preliminary DC S/N ratio studies.-It has been noted previously that the ion detector was a simple Faraday cup. In order to obtain sufficient charge gain for ion counting, a 14-stage electron multiplier was installed at the beginning of this work. Initial studies of S/N ratio were begun on a dc basis, i.e., the output of the electron multiplier was measured by an electrometer.

These early studies uncovered a source of noise in the output spectrum not previously encountered. Further investigation established that the CCIS was the predominant source of this background noise and the noise current was nearly linearly related to the anode potential of the CCIS.

In an effort to uncover the cause of this noise a number of potential noise sources were considered and investigated. Among these was the strong electron flux which was discovered emerging from the ion source during earlier feasibility studies. Photons are also known to be produced within the discharge. Accordingly, an experiment was performed to define whether or not the noise source was predominantly photons or charged particles.

It will be recalled that the two ion source cathodes ($K_1$ and $K_2$) are electrically isolated from the grounded entrance aperture of the quadrupole. This permits the retardation of ions prior to their entrance into the quadrupole. It had been shown in the development of the CCIS/Quad, that such retardation is necessary to achieve optimum quadrupole resolution.

As the value of the retardation potential ($V_R$) was increased from zero to 250 volts, the ion current of all mass peaks, including the "on blast" (all ions unresolved at M/e = 0), decreased as anticipated. The baseline noise current however increased. For this experiment, a negative retarding voltage was applied simultaneously to the two CCIS cathodes ($K_1$ and $K_2$) so that the potential between the exit cathode, $K_2$ and quadrupole entrance aperture (grounded) is a retarding potential for ions. At the same time, the true anode-to-cathode potential of the CCIS is increased by an amount equal to $V_R'$ and therefore the noise current also increases. Subsequent experiments were conducted using both positive and negative values of $V_R$ in the range of 0 to 500 volts. The true anode-to-cathode voltage was held constant. In these experiments, no appreciable change in the baseline noise value was observed for either positive or negative values of $V_R$.

Since the noise level was not observed to change in response to a wide range of external fields which are both retarding and accelerating potentials for charged particles, it is concluded that the noise source is largely photons produced within the ion source proper. These photons then are transmitted along the axis of the quadrupole and subsequently stimulate the first dynode of the multiplier.

An attempt was made to reduce the photon background within the source based upon a very simple assumption. It was postulated that soft x-rays

might be produced by energetic electrons within the discharge. These electrons, upon striking the blunt end of the cathode stub, would produce x-ray photons visible from the multiplier end of the analyzer, since the end of the stub fills the major portion of the cathode exit aperture as seen by the multiplier. Consequently, the stub of $K_1$ was removed and replaced by a thin-walled tube of the same diameter and length as the stub. In this configuration the multiplier "sees" only the small annulus of the stub area. In the resultant experiment, the operating and vacuum conditions were maintained as close to the previous conditions as possible. The results are shown in figure 14. This figure shows the observed baseline current is no longer discernable ($< 1 \times 10^{-14}$ amperes), under conditions similar to those of the solid stub. Moreover, there is no apparent increase in this background as the true anode voltage is increased ($V_R$ increasing).

The present speculation is that the photons are not soft x-rays resulting from electron impacts but are probably identical to the photons observed and photographed by Feakes, et al. (ref. 9). Perhaps, by modifying the cathode stub, the visible cathode glow is prevented from establishing itself around the end of the stub and the resultant light surrounds only the outer surface of the tubular stub. Only a small portion of this glow would be visible to the multiplier because the diameter of the tubular stub and ion exit aperture are nearly identical.

With these investigations the preliminary dc S/N ratio studies were concluded. The unit was then set up for ion counting studies in accordance with the block diagram previously shown.

Initial investigations.-The initial phase of the ion counting investigations centered on a study of signal and noise pulse height distribution curves

of the integral type explained in the previous section. During these experiments, the CCIS anode voltage was maintained at values of 1000 volts or less. The cathode stub of $K_1$ was solid, with a rounded tip as noted previously. This was later removed and the tubular stub substituted. A magnet of 850 gauss was used, and the mass spectra of the system residual gases were used for study purposes. Typically, the ultimate system total pressure was in the low $10^{-11}$ torr (nitrogen) range, unless indicated otherwise. The predominant residual gases present were $H_2$, CO, and $CO_2$ with smaller amounts of He, $CH_4$ (methane series), neon and argon. No residual constituents were observed above mass 44 ($CO_2$) and therefore, noise measurements were made at mass 50. The electron multiplier was operated near -2700 volts, a value slightly less than the recommended one of -3000 volts (with respect to ground). The non-overloading amplifier gain controls were set arbitrarily to produce ion counting rates of the order of $10^4$ to $10^5$ counts per minute for the argon (mass 40) peak.

The major purpose of these early investigations was to learn more of the pulse height distribution characteristics of signal (ion) and noise pulses. If the two distribution curves are essentially the same function with the same <u>average</u> pulse amplitude, discrimination against noise on an amplitude basis would be impossible without incurring a similar discrimination against signal pulses. Briefly then, the S/N ratio would be independent of discriminator setting. On the other hand, if the average signal pulse amplitude is larger than the average noise pulse, some amplitude discrimination is possible. It is assumed in this case that the distribution curves of signal and noise are similar. Finally, if the average pulse heights of signal and noise is significantly different (signal > noise) <u>and</u> the distribution of noise pulse heights

is narrower than the signal distribution, the S/N ratio will increase as the discriminator amplitude level is increased.

Counting S/N vs. CCIS operating parameters.-The CCIS has four operating parameters which affect the instrument S/N ratio. These parameters are:

(1) Ion Retardation Voltage

(2) Anode Voltage

(3) Magnetic Field

(4) Total Pressure within the Ion Source.

The effect of each of these variables on S/N ratio has been studied individually and in combination with one another and the results are summarized in the following paragraphs.

Counting S/N ratio vs. ion retardation voltage: It has been shown that the dc and counting noise level is independent of the ion retardation voltage. The signal is, however, directly dependent thereon.

Counting S/N ratio vs. anode voltage: A distinct maximum is observed in the S/N ratio due to the combined effects of $V_R$ and $V_A$. The signal counting rate and S/N ratio decrease very rapidly for anode voltages < 1000 volts because the chosen value of $V_R$ (-100 volts) accentuates the decline in sensitivity due to the retarding process. Above 1800 volts the sensitivity of the source begins to saturate, whereas photon noise is still increasing rapidly. Thus, we see that when the combined effects of both $V_R$ and $V_A$ are examined that the counting S/N ratio appears to be maximum at a considerably higher anode potential and a higher sensitivity than expected.

In brief, the anode voltage for an optimum trade-off of sensitivity and S/N ratio appears to be very nearly 1000 volts. While the S/N ratio may be larger at 500 volts and zero retarding voltage, the sensitivity reduction is

not tolerable. The improved sensitivity at 1000 volts is certainly worth the small reduction in S/N ratio.

Counting performance vs. magnetic field: The general performance of the ion counting detector and the spectrometer have been investigated as a function of magnetic field. In this work, two magnets were used which were physically the same but were different in field strength. One magnet was 850 gauss and the other was 1133. The field strength is measured at the center of the magnet's axial hole.

Although it has been shown that the stray magnetic field associated with the stronger magnet does affect multiplier gain, the S/N ratio for the same value of noise (1 cps) and the counting efficiency are not significantly changed. Therefore, the stronger magnet was used during all subsequent investigations.

Counting performance vs. total pressure: The last remaining source parameter to influence ion counting performance is the pressure of gas within the ion source.

It has already been noted that background photon noise in the ion source is dependent on the total "pressure" within the ion source. Actually, the intensity of the photon emission is related to the total ionization occurring within the discharge. This, in turn, is related to the number density of each species present and to the ionization efficiency of each species. It is particularly important to recall these facts in the case of the present discussions, because if the relative abundance of the species change as the total pressure changes, the effect on the noise level will be two-fold; the noise will be dependant on both total pressure and on the species. To investigate the relationship between photon noise rate and source pressure, an

experiment was planned which would relate the noise rate to the ion current measured at cathode $K_1$ ($I_{K1}$). This current is related to the ion production rate within the discharge. However, difficulties were encountered in the form of an excessive leakage current at the $K_1$ terminal. This current was larger than the corresponding $I_{K1}$ currents at the lowest pressures used in the investigation ($3 \times 10^{-12}$ torr). As the pressure was increased within the ion source, $I_{K1}$ gradually became large enough to measure but at this point, the photon counting rate became too large to measure on the counting equipment.

Maximizing detector S/N.-The operating conditions of the electron multiplier also influence the overall S/N ratio achieved by the instrument. Of equal importance is the collection efficiency of the detector since this effects the sensitivity of the instrument.

In summary, the following observations have been made regarding maximizing the ion detector S/N ratio:

(1) The secondary emission ratio, $\gamma$ is important in determining S/N ratio, but the limitations on improvement by increasing $\gamma$ are predominantly electronic in nature.

(2) The most important increase in S/N ratio should be the result of locating the multiplier off-axis so that it is "blind" to photons. Careful design is important in order to achieve high ion collection efficiency for all masses.

(3) The sensitivity of the detector to random gain changes in the multiplier is much reduced by the use of counting techniques.

## Conclusions

The use of counting techniques promises major improvements in S/N ratio, detector stability and measurement accuracy of UHV total and partial pressure

measuring instruments. Although the present arrangement is not optimum, it has been shown that a detector can be operated with counting and collection efficiencies approaching 100%. These efficiencies have been achieved using an in-line quadrupole analyzer-detector system which represents a non-ideal situation for photon noise background rejection. For a magnetic sector analyzer with its excellent noise and signal geometrical separation, the technique may be applied immediately to improve stability and S/N ratio. For axial-aligned r-f analyzers such as time-of-flight and quadrupole instruments, the photon background should be reduced by using an electrostatic deflector together with an off-axis multiplier to divert and deflect the ions. These techniques have already been applied to dc current detectors.

Finally, ion counting techniques may also be employed to continuously monitor the gain of the electron multiplier in conventional dc ion detectors if the latter type of detector is preferable for routine analysis.

## II. INSTRUMENT DEVELOPMENT SYSTEMS

The success of the gage development program at LRC has been due in large part to the extensive test facilities that have been developed for use in ultra high vacuum experiments. While the laboratory contains many general vacuum systems, it is the systems especially designed for gage development that have permitted the greatest contributions to be made. In the following section, three of these systems will be described. While the systems differ in many respects, they have two features in common: (1) They were especially designed for vacuum gage development, (2) they can reach the $10^{-13}$ torr range or lower.

The first of the systems to be described is the simplest of the systems, and is used for general and "first experiment" work when it is desired to be able to install and remove gages easily. The system is shown in figure 15 with a number of gages installed, including some of the early double ended models of the buried collector gage. The system is also shown schmetically in figure 16 and is an improved version of the system reported by Outlaw (ref. 4). The system uses a combination of turbomolecular, ion and titanium sublimation pumping. In a typical procedure, the turbomolecular pump is used as a roughing pump down to $1 \times 10^{-8}$ torr where bakeout, at temperature up to 300°C, are begun. Turbomolecular pumping is continued throughout the bake cycle. After bakeout, the turbomolecular pump is isolated from the system and further pumping is done by ion pump and $LN_2$ shrouded titanium sublimation. The deposition per filament flash (1 minute at 45 amps) is approximately $2 \times 10^{-6}$ grams/cm$^2$. This gives, for the system, a pumping speed of approximately 1000 liters/sec. for hydrogen, and corresponding speeds for other gases. The ion pump supplements the pumping for gases not readily pumped by

titanium. Figure 17 is a typical pump down curve for the system. Bake time is variable and is determined by the amount of $H_2O$ remaining in the system as measured by RGA. After reaching low pressures the system is kept down by flashing the titanium filaments as needed. It has been found necessary to sublimate (45 amps for 1 minute) once every 24 hours for pressure in the $10^{-10}$ torr range, but for pressures below $1 \times 10^{-11}$ torr, once every 72 hours is sufficient.

The second system to be described is shown in figure 18. This system is much more complex than the previous system as can be seen from the schematic view shown in figure 19. The system is a triple walled system with the outer wall acting as a guard vacuum and structural support. The second wall is a $LN_2$ liner and provides a vacuum and thermal barrier for the inner chamber. The inner chamber wall is 3 mm thick copper which forms a working volume 46 cm in diameter and 61 cm in length. Pumping is through a port 13 cm in diameter in one end of the chamber. This port is a knife edge orifice so that the conductance is accurately known. With a known flow rate of He gas into the chamber, and the exit flow rate known, the pressure in the chamber can be accurately established. Helium gas is used for experiments, since the working chamber is cooled by gaseous He to as low as $10^{o}K$, and gases other than He are pumped by the chamber walls. Figure 20 is an internal view of the system showing the working chamber with the gage mounts and the electrical feedthroughs. Also, at the back of the work chamber may be seen the ion source of a quadrupole mass spectrometer.

A typical pump down curve is shown in figure 21. Total time from start up to base pressure, including bake-out time, is of the order of 16 hours. Although base pressures in the working chamber are $10^{-14}$ torr or below, exper-

iments are limited to the $10^{-13}$ torr range to avoid background gases and due to limitations in the accuracy of the gas inflow measuring devices. The background pressure is given as below $10^{-14}$ torr since all gages so far tried reach their x-ray limits or extinguish (in the case of the Redhead gage, readings of $2 \times 10^{-14}$ torr were obtained which appeared to be a background current, but there was evidence that the gage was operating) at chamber wall temperatures of 15-20°K, whereas the final chamber temperature reaches 10°K.

The third system is a molecular beam system shown in figure 22. Again the multiple wall approach is used, proceeding from the outer structural wall, an $LN_2$ liner, a gaseous He liner, and finally to the LHe working chamber. Figure 23 is a simplified schematic drawing of the system. Shown are the essential parts needed to describe the basic operation of the system. A pressure in (2) is measured by a primary standard (1) whose calibration is traceable to the National Bureau of Standards. From (2) the gas bleeds, in molecular flow, through a calibrated porous plug (3) into a molecular furnace (4). The temperature of this furnace is carefully controlled so that the density of the gas may be accurately calculated. A diffuse gas issues from the near-perfect orifice (8) in a cosine distribution. The core of this gas effusion (9) proceeds down the work tunnel as a molecular beam, the remainder of this gas being removed by LHe cooled strippers. (As opposed to the operation of the XHV system, the working gas is not Helium, so that it <u>will</u> be pumped by the LHe surfaces). A gage, mounted at (12) is thus exposed to the molecular beam of gas where density is known to within ±5%. The background pressure in the working chamber may be ignored for experiments down to the $10^{-14}$ torr range due to the high capture probability of the LHe surface for test gases such as nitrogen and argon. Figure 24 shown the furnace with its orifice.

Figure 25 shows the mounting arrangement of the furnace onto the system: It can be shown that the density of the beam is:

$$\eta_b = \frac{2}{3}\left(\frac{r_a^2}{\ell}\right)\eta_f$$

where: $\eta_b$ = molecular density of beam

$r_a$ = radius of furnace exit orifice, cm

$\ell$ = distance between orifice and gage, cm

$\eta_f$ = molecular density of furnace

The diameter of the beam at the gage station (12) is such that a nude gage is completly within the beam. However, for a tubulated gage a correction needs to be made due to restriction and conductance of the gage tubulation. The experiments with tubulated gages are therefore carried out with the gages in a thermal equilibrium enclosure (fig. 26). The mounting arrangement of the enclosure onto the chamber is shown in figure 27. The steady state molecular density in the gage enclosure may be shown to be

$$\eta_e = \frac{\bar{V}_f}{\bar{V}_e}\frac{r_a^2}{r_a^2 + r_e^2 + \ell^2}\eta_f$$

where: $\eta_e$ = molecular density in enclosure

$\bar{V}_f$ = average molecular speed in furnace, cm per sec.

$\bar{V}_e$ = average molecular speed in enclosure, cm per sec.

$r_a$ = radius of furnace orifice, cm

$r_e$ = radius of enclosure orifice, cm

$\ell$ = distance between orifices, cm

$\eta_f$ = molecular density in enclosure

The derivation of this and the previous equation may be found in the paper by Smith (ref. 10).

By using two positions of gage mounting, and by varying the source pressure, the range of known density, within ±5%, is from $5 \times 10^{-13}$ to $2 \times 10^{-8}$ torr without the enclosure, and $2 \times 10^{-10}$ to $2 \times 10^{-6}$ torr with the gage enclosure. The upper limit of use in fixed by molecular flow considerations, and the lower limit is determined by the accuracy of the primary standard used to measure upstream pressure. If the requirement to ±5 percent accuracy is relaxed, then the system may be used into the low $10^{-14}$ torr range.

## III. CALIBRATION FACILITIES

It must be recognized that the best measurement techniques, advanced gages, and elaborate development programs are made relatively useless unless adequate calibration facilities are available. It is unfortunate that the vacuum area suffers from a lack of primary standards, and that secondary, or relative, standards must be used over a portion of the range, with the lower end having no standards at all. This lack of standards has been recognized by LRC for several years as one of the major problems in vacuum measurements. Accordingly, considerable effort has been made to provide in-house calibration facilities, and to support both in-house and contract efforts to improve, extend the range, and develop new standards.

Two major facilities have been provided for in-house calibration work. Both systems are based on flow division and Knudsen flow laws to provide repeatable working standards. Even though it must be recognized that this approach is not yet acceptable as a primary standard, the method provides a repeatable working standard. The more advanced of the two systems is the molecular beam system previously described. While not originally intended to be used as a calibration facility, its usefulness in this area has led to the adoption of the system for gage calibration work from $10^{-10}$ to $10^{-13}$ torr. The fact that the molecular beam can operate in the $10^{-7}$ range provides an overlap with the other system which operates as low as $10^{-9}$ torr. The principle system operates over the range of $1 \times 10^{-4}$ to $1 \times 10^{-9}$ torr with a maximum error of less than ±6 percent.

This system (fig. 28) consists of a gas flow rate generating and measurement flowmeter and vacuum system to which the gages to be calibrated are attached. The vacuum system consists of two chambers; a gas flow divider

chamber and a gage calibration chamber, with each chamber being pumped by a 500-liter/second ion pump and a titanium sublimation pump. In addition, the gage calibration chamber is pumped by a liquid nitrogen cryosurface onto which titanium vapor is deposited for increased pumping efficiency. Orifices (shown in the schematic drawing at 1 and 3 of fig. 29) provide for a constant volumetric rate of gas removal from the chambers into the pumping systems. The orifice at 4 introduces a pressure attenuation between the flow divider chamber and the gage calibration chamber.

To perform vacuum gage calibrations in the range of $2 \times 10^{-7}$ to $1 \times 10^{-4}$ torr gas is admitted directly into the gage calibration chamber through the flow divider chamber bypass. The valve positions are as follows:

| Valve | Position |
|---|---|
| A | Closed |
| B | Open |
| C | Closed |

For gage calibrations in the range of $1 \times 10^{-9}$ to $2 \times 10^{-7}$ torr, the calibration gas flow rate is attenuated by passing it through the flow rate division chamber and into the calibration chamber. The valve positions are as follows:

| Valve | Position |
|---|---|
| A | Open |
| B | Closed |
| C | Open |

The calibration gas flow rate entering the calibration system is both generated and measured by the constant pressure gas flowmeter (fig. 30). This flowmeter contains a valve for controlling the evacuation rate of the

flowmeter and another valve for controlling the calibration gas inlet rate to the flowmeter. These valves are necessary for the protection of the sensitive differential pressure meter diaphragm and are normally closed during flowmeter operation. A leak valve is used to control the gas flow rate into the vacuum system. A 0- to 800-torr manometer is utilized for measuring the calibration gas supply pressure in the flowmeter. The sensitive differential pressure meter is used to measure the differential pressure between the reference side and the variable volume side of the flowmeter and a bypass valve is provided to permit equalization of flowmeter pressure prior to a flow rate measurement and also to isolate the reference side from the variable volume side during a flow rate measurement. A flow rate measurement is performed by opening the leak valve until the approximate desired pressure is established in the calibration chamber as indicated by an ionization gage. After equilibrium conditions are established in the calibration chamber, the flowmeter bypass valve is closed. As gas is allowed to flow from side A, the pressure is reduced. The internal volume of side A is reduced by mechanically inserting a cylinder of known cross-sectional area into the flowmeter at a rate which produces a zero differential pressure across the diaphragm of the differential pressure meter. The ratio of volumetric cylinder change to time is proportional to the gas flow rate into the calibration chamber.

This calibration system is bakeable to 525°K. The ultimate pressure attainable in the gage calibration chamber is approximately $3 \times 10^{-11}$ torr. This ultimate pressure is on the order of 2 decades of pressure lower than the minimum calibration point of $1 \times 10^{-9}$ torr. This assures that the calibration gas comprises approximately 98 percent of the total gas pressure at $1 \times 10^{-9}$ torr, thus eliminating heterogeneous gas effects on the output of the

ionization gage being calibrated. A detailed analysis of this system has been made by Kern (ref. 11) which gives considerations of orifice sizes, pumping speeds, gage effects, and which calculates the maximum uncertainty in the knowledge of the pressure in the calibration system as ±5.5 percent.

A second system, with a range of $10^{-3}$ to $10^{-7}$ torr is also available. Due to its similarity to the above system, no details will be presented.

In the area of absolute standards, work has been undertaken to provide primary standards which function below the range of the McLeod gage, which we take as $1 \times 10^{-5}$ torr. Two separate approaches have been taken; one is a vane type gage, the second is a gas-metal system.

The Vane gage is being developed as an absolute pressure standard under a co-operative program between LRC/NASA and the National Bureau of Standards. Resolution of the gage is $10^{-11}$ torr, which gives a 10% error at $10^{-10}$ torr and 1% or less above $10^{-9}$ torr. Since the gage actually measures force per unit area on a movable vane it is a true pressure standard. Application of this principle in 1935 by Hickman, et al., (ref. 12) resulted in a gage with reproducibility of better than $3 \times 10^{-5}$ torr. One such instrument with a quartz fiber furnishing the restoring force, showed high sensitivity and encouraged further study of the gage (ref. 13).

Methods of measuring the force on the vane and the position of the vane are now such that the ultimate limit of such a gage may be the Brownian motion, as is the case with some sensitive galvanometers. Calculations indicate that if this limit is attained in a vane gage, the gage could be used into the $10^{-11}$ torr range. Other limiting factors, such as radiation pressure due to temperature differences and optical readout uncertainties, appear to be such

that, with proper control, these uncertainties can be reduced below the Brownian motion limit.

An advantage of a gage of this type is that the system being measured is not greatly disturbed with high temperatures, nor with strong electric and magnetic fields as is the case in various ionization gages. Of even more importance is the fact that if the correlation between the force on the vane and the pressure at the gage inlet can be derived, the gage would become an absolute measuring instrument, i.e., its calibration would be directly in terms of fundamental quantities. This problem is being studied by the Monte Carlo method. Preliminary results show that such a correlation can be obtained (ref. 14).

The gage is essentially a torsional microbalance in which the force of molecular bombardment on the vanes is counteracted by a calibrated nulling force. Tubulations direct the gas to the pressure side of two vanes suspended as shown in figure 31, and the entire assembly is contained in an evacuated chamber. For simplicity, the restoring force is shown as a torsional fiber; however, electrostatic and electromagnetic restoring forces are being considered. The photograph of the NBS gage in its present form shows some of the versatility incorporated into the frame work (fig. 32). The port positions are adjustable and the type of suspension is not restricted. Also, a balanced symmetric arrangement makes it possible to have a reference pressure on one side of the vanes which is different from the guard pressure which surrounds the gage.

In a torsional balance with one (rotational) degree of freedom, the mean square displacement for the system in thermal equilibrium is: $\overline{\theta^2} = \frac{kT}{S}$, in which T ($\cong$ 300 K) is the temperature, S is the torsional constant of the

suspension, and k is Boltzann's constant ($\cong 1.4 \times 10^{-16}$ erg/K). Sensitive galvanometers are now commercially available with a torsional constant of about 0.1 dyne cm/radian, so that a reasonable estimate of the RMS displacement due to thermal agitation seems to be:

$$\theta_{RMS} \cong 6.5 \times 10^{-7} \text{ radians.}$$

The pressure, p, corresponding to a displacement, $\theta$, on the two vanes of area A separated by a distance d, is given by

$$p = \frac{S\theta}{Ad} .$$

Design values of A = 1.3 $cm^2$ and d = 7.6 cm give as the Brownian motion limit in terms of RMS pressure,

$$P_{RMS} \cong 7 \times 10^{-9} \frac{\text{dyne}}{cm^2} \cong 5 \times 10^{-12} \text{ torr}$$

The probability of a deflection greater than $\theta_{RMS}$ is about 30%; greater than 2 x $\theta_{RMS}$ about 5%; and greater than 3 x $\theta_{RMS}$ is about 0.1%. Therefore, with short observation times, a deflection of 2 x $\theta_{RMS}$ should be detectable so that we may say the Brownian motion limit is less than $2 \times 10^{-6}$ radians which corresponds to about $1 \times 10^{-11}$ torr.

If the temperature of the walls facing opposite sides of a vane are not equal, a pressure difference due to radiant energy will result amounting to:

$$\Delta p = \frac{4\sigma}{3c} (T_2^4 - T_1^4)$$

in which $T_1$ and $T_2$ are the two temperatures, $\sigma$ is the Stefan-Boltzmann constant ($5.67 \times 10^{-5}$ erg/$cm^2$ sec $K^4$), and c is the speed of light ($3 \times 10^{10} \frac{cm}{sec}$). If $T_2$ is greater than $T_1$ by a small amount $\delta$, then we have:

$$\Delta p \cong 1 \times 10^{-14}\ \delta T^3,$$

so that, for a temperature difference of 1K at 300K,

$$\Delta p \cong 3 \times 10^{-7}\ \frac{\text{dyne}}{\text{cm}^2} \cong 2 \times 10^{-10}\ \text{torr}.$$

It is therefore apparent that pressure uncertainty from this source can be easily reduced below the thermal agitation limit by temperature control of about 0.05 K which is not difficult to achieve.

Optical sensing of angular position in some commercially available sensitive galvanometers is better than $1 \times 10^{-6}$ radians which is below the estimated Brownian motion limit of the gage.

Preliminary studies of capacitance methods of damping out oscillations and of furnishing the necessary restoring forces have indicated that control is attainable with reasonable voltages and circuitry.

For example, calculations for a configuration similar to the quadrant electrometer and with physical dimensions compatible with the present framework, show that the pressure range up to $10^{-7}$ torr would require an emf of about 1 volt across the capacitor plates; with 100 volts, the gage could be operated into the $10^{-3}$ torr range.

The theoretical limits discussed here lead to an uncertainty far below any available absolute gage. There are practical problems which must also be overcome such as mechanical isolation from vibrations, etc.

The second approach to a primary standard is the metal-gas system. In this case an investigation had been made of the erbium-hydrogen binary system for use as a source of hydrogen gas at a known pressure.

This technique is a new and unique approach to setting up partial-pressure standards by which calibrations of ionization gages can be conducted in a much simpler and more reliable manner.

The selection of hydrogen as the gas to produce a standard is appropriate because it is probably the most difficult of all the gases with which to obtain accurate reduced-pressure measurements. If this gas can be pressure standardized, the other active gases such as oxygen and nitrogen will be much simpler to develop at a later date. Particularly with the ionization gage, measurements of hydrogen reduced pressures are beset with many problems. Foremost of the problems is reaction of hydrogen with the hot tungsten filament to produce atomic hydrogen. This dissociation is accelerated as the temperature increases. The reaction is further affected by the condition of the surface of the tungsten. If other gases are absorbed, the reaction rate is modified, accordingly. Various auxiliary reactions can occur. Thus, it is impossible to obtain reproducible results because the temperature and surface condition of the tungsten filament are not subject to control. The technique relies on the thermodynamic properties of metal-gas systems as a basis for its success. The thermodynamic properties of these systems are fixed and immutable under certain controllable conditions. The property of interest is the reduced pressure of the gas over the solid, which varies as a function of temperature and composition. The manner in which it varies can be determined experimentally and fit to an analytical relationship. Thus, by using a primary standard to measure the pressure as a function of temperature and composition, the system itself becomes a standard. One simply has to establish the temperature and the composition, and the reduced pressure is exactly reproduced. This in turn can be used as a secondary standard to calibrate

other gages. The advantage is that the thermodynamic properties will not change with time or are they affected by other influences that usually affect other pressure standards. By selecting a metal-gas system with a two-phase field, the system becomes an even simpler and more reliable standard. Gibbs Phase Rule states that in such a binary metal-gas system, the appearance of two phases rather than one causes a loss of one degree of freedom. Such is actually the case wherein the degree of freedom which is lost is pressure. Thus, at a certain fixed temperature, the pressure remains constant no matter what the composition is, as long as the solid system remains in the two-phase field.

A specific working example of a reduced-pressure standard was demonstrated in the determination of the thermodynamics of the erbium-hydrogen system, which established that the erbium-hydrogen system had potential as a secondary partial-pressure standard. It remained to refine the thermodynamic characteristics in the two-phase region. The pressure-temperature-composition relationships in the erbium-hydrogen system were determined experimentally with a Sievert's apparatus. The procedure employed to obtain the pressure-temperature-composition relationships was to develop experimentally a family of isothermal curves of composition versus pressure. Figure 33 shows the family of isotherms for the Er-H system. The solubility relationships can be deduced from these isotherms. As the first amounts of hydrogen are added to erbium metal, the pressure increases. At saturation of the metal solid solution, the pressure reaches a plateau. Additional hydrogen initiates the formation of the dihydride phase as the pressure remains constant in this two-phase region. As can be observed, this plateau region is quite extensive. In accordance with the Phase Rule, the appearance of another phase signifies

the loss of one degree of freedom, namely that pressure is constant. The pressure again rises from the plateau at the boundary of the single-phase dihydride region. For the purposes of this research study, the plateau region is the center of interest.

The plateau equilibrium reduced pressures were plotted as $\log_{10}P$ versus the reciprocal of the absolute temperature. A straight-line relationship resulted and was quantitatively determined by computer least-square analysis. The following equilibrium-dissociation-pressure equation which was obtained is:

$$\text{Log}_{10}\rho \text{ (Torr)} = -\frac{11{,}500 \pm 70}{T} + 10.57 \pm 0.07$$

where: $\rho$ = equilibrium hydrogen pressure, Torr

$T$ = temperature, $^{o}K$

The above work, which was reported by Lundin (ref. 15) reached the following conclusions:

1. Once the dissociation pressure equation is established and standardized, one can calculate the corresponding temperature setting for any desired pressure. Then, by adjusting the temperature to the appropriate value, the pressure can quickly be attained.
2. There is no hysteresis in the hydrogen pressure. The system can be cycled any number of times, and the pressure will return to the value as prescribed by that specific temperature.
3. In temperature range studied, pressure equilibrium is very rapid.
4. The equilibrium pressure for each respective temperature is independent and unaffected by the volume or geometry of the system. There is an exception to this when the composition is shifted off the

plateau by having a very small hydride specimen and a very large system.

5. The partial-pressure plateau in the two-phase region is very extensive, and shifts in overall hydrogen composition do not affect the pressure at any specific temperature.
6. Contamination from outgassing or inleakage does not seriously affect the equilibria established according to the dissociation equation.
7. A metal-gas system such as the erbium-hydrogen system will establish accurate reduced pressures which bracket the manometer, the McLeod gage, and the ionization gage in a continuous manner.
8. There is no reason to believe that a standardized dissociation equation for such a system prepared in the higher pressure range where good primary standards exist could not be extrapolated to lower pressures with a high degree of confidence in accuracy. The following table gives approximate values for some of the calculated hydrogen reduced pressures in the high- and ultrahigh-vacuum region.

Extrapolated Hydrogen Reduced Pressures

| Temperature, $^{o}C$ | Pressure, torr |
|---|---|
| 450 | $4.65 \times 10^{-6}$ |
| 350 | $1.17 \times 10^{-8}$ |
| 300 | $2.70 \times 10^{-10}$ |
| 250 | $3.70 \times 10^{-12}$ |
| 200 | $9.30 \times 10^{-15}$ |

9. One distinct advantage of this technique is that an in situ calibration can easily be devised for any ultrahigh vacuum apparatus,

where an immediate calibration of the measuring apparatus can be available.

10. The system is inexpensive to build and relatively simple in design and use. The temperature range can be easily attained and measured with commercially available thermocouples.
11. The erbium can be hydrided to the appropriate composition, removed to air, and transported to another system without affecting its dissociation relationships.
12. Other metal-hydrogen systems exist which give somewhat different equilibria. This would give a lot of flexibility in selecting the appropriate temperature and partial pressures for the specific application.
13. The range of temperatures over which the wide spread of pressures exist are easily measured. A chromel-alumel thermocouple can be employed which has a very high EMF per unit temperature increases. Also, standard materials of construction for the furnace chamber can be employed because the highest temperatures required are not at all severe.
14. The simulation of any hydrogen reduced pressure atmosphere is feasible in any type of chamber or system by simply placing a small heating source and a prehydrided specimen in the chamber with a means for measuring the temperature of the hydride.

The success of the early work has encouraged an in-house program to compliment further work by Lundin. The in-house program is aimed at providing in-situ calibrations in the UHV region. The experimental apparatus is shown in figure 34 mounted on one of the turbomolecular-titanium sublimation

systems. The apparatus is shown schematically is figure 35. Present work is being carried on in the $10^{-10}$ - $10^{-12}$ torr range. There is, however, insufficient data to present results at this time.

## CONCLUSION

In conclusion, this paper has attempted to present an overall picture of the work being done and supported by the Langley Research Center of NASA to improve the measurement capabilities in simulated space environments. It has not been possible to present all of the work, notable exceptions being thermal transpiration studies and gas-surface interaction experiments. However, it is hoped that sufficient information has been presented to firmly establish the interest in and support of space simulation measurements by the Langley Research Center.

## REFERENCES


1. Smith, A. and Melfi, L. T., Jr.: Construction and Evaluation of a Nude Fast-Response Cold-Cathode Ionization Gage, NASA TN D-3266 National Aeronautics and Space Administration, Washington, D. C. February 1966.

2. Clay, F. P. and Melfi, L. T., Jr.: J. Vac. Sci. Technology 3, 167 (1966).

3. Melfi, L. T.: J. Vac. Sci. Technology, 6, 322 (1969).

4. Outlaw, R. A.: J. Vac. Sci. Technology, 3, 352 (1966).

5. Helmer, J. C. and Hayward, W. H.: Review Sci. Instruments, 37, 1652 (1966).

6. Brock, F. J.: Research and Development Program on Orbitron Ultra-High Vacuum Gages. Final report on contract NAS1-5347-7, NASA CR-1479, November 1969.

7. Schwarz, H. A.: Quadrupole Ionization Gage, Fourth International Vacuum Congress, Manchester, England, April 1968.

8. Torney, F. L., et. al.,: A Cold-Cathode Ion Source Mass Spectrometer Employing Ion Counting Techniques, final report on contract NAS1-5347-8, NASA CR-1475, October 1969.

9. Feakes, F.; Muly, E. C.; Brock, F. J.: Extension of Gage Calibration Studies in Extreme High Vacuum, NASA CR-904, October 1967, pp 118-129.

10. Smith, A.: Analysis of a Molecular Beam Known Pressure Source, NASA TN D-5308, July 1969.

11. Kern, F. A.: NASA-LRC internal memorandum.

12. Hickman, K. C. P., et. al.: Ind. and Engr. Chem. Anal. Ed. 264 (1937).

13. Ruthberg, S.: National Bureau of Standards, private communication.

14. Thomas, A. M.: J. Vac. Sci. Technology, 5, 187 (1968).

15. Lundin, C. E.: The Use of Thermodynamic Properties of Metal Gas Systems as Reduced Pressure Standards, NASA CR-1271. January 1969.

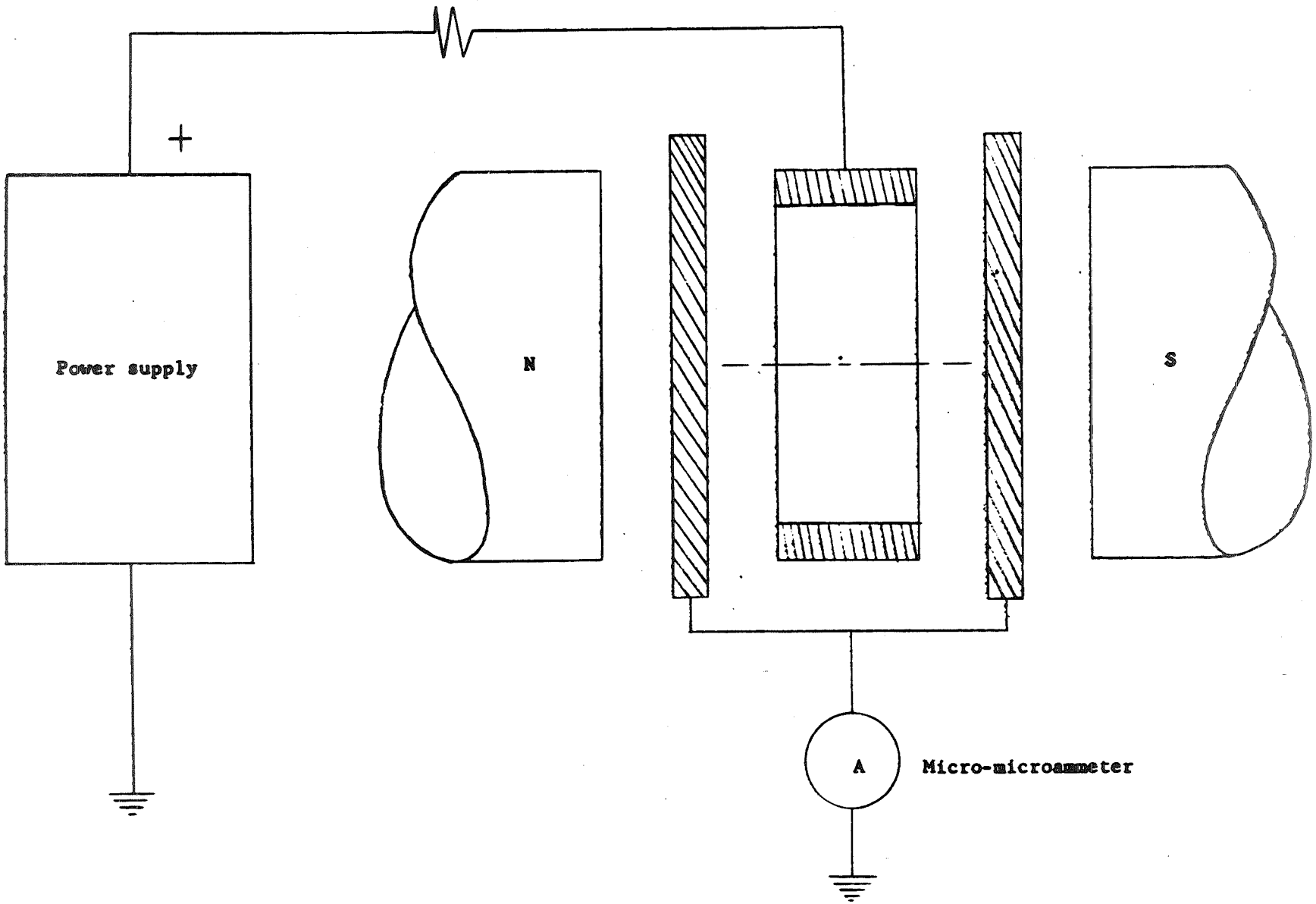


Figure 1.-Cold-cathode gage schematic.

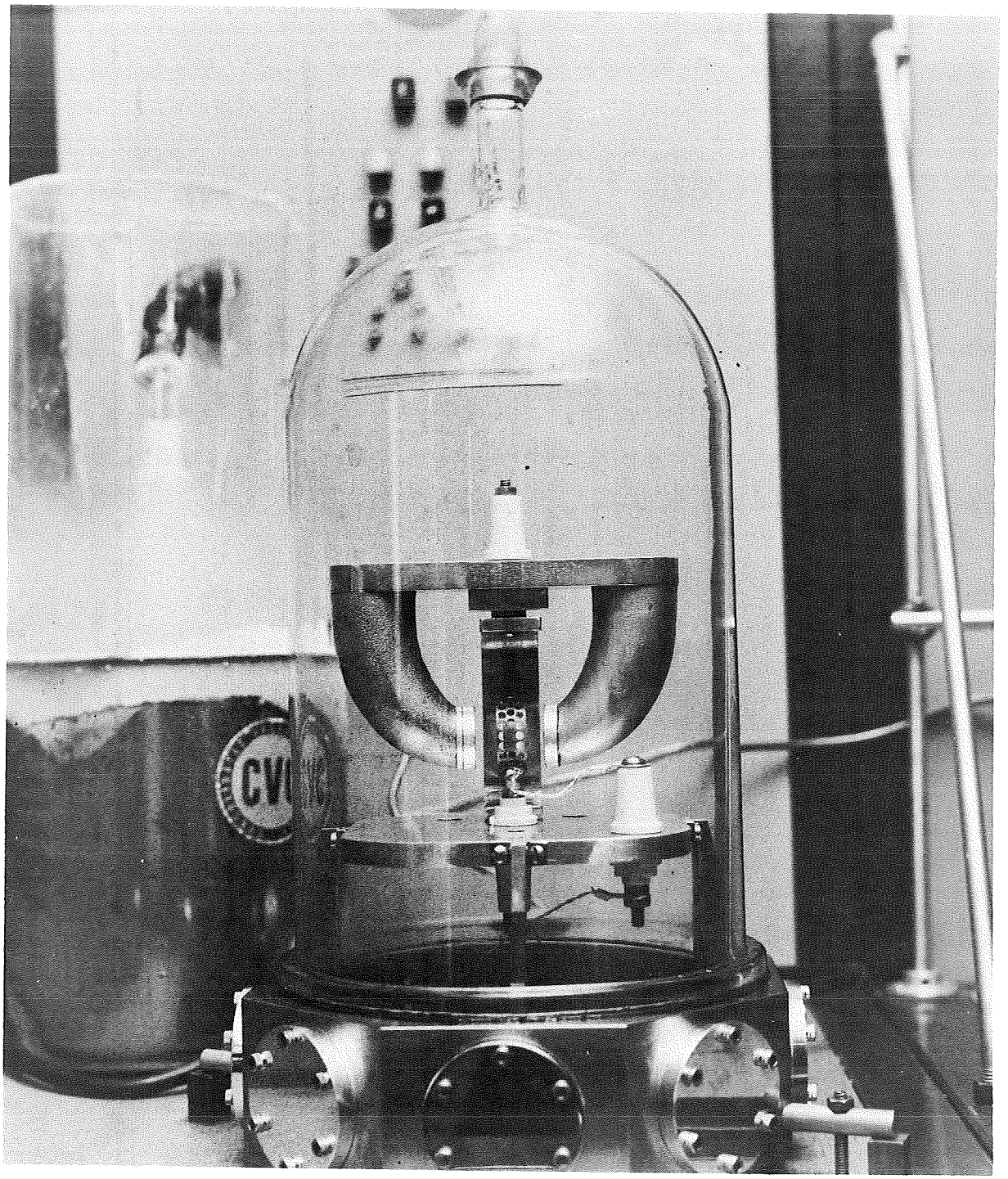

Figure 2.-Arrangement of apparatus in vacuum chamber for cold-cathode gage time response experiments.

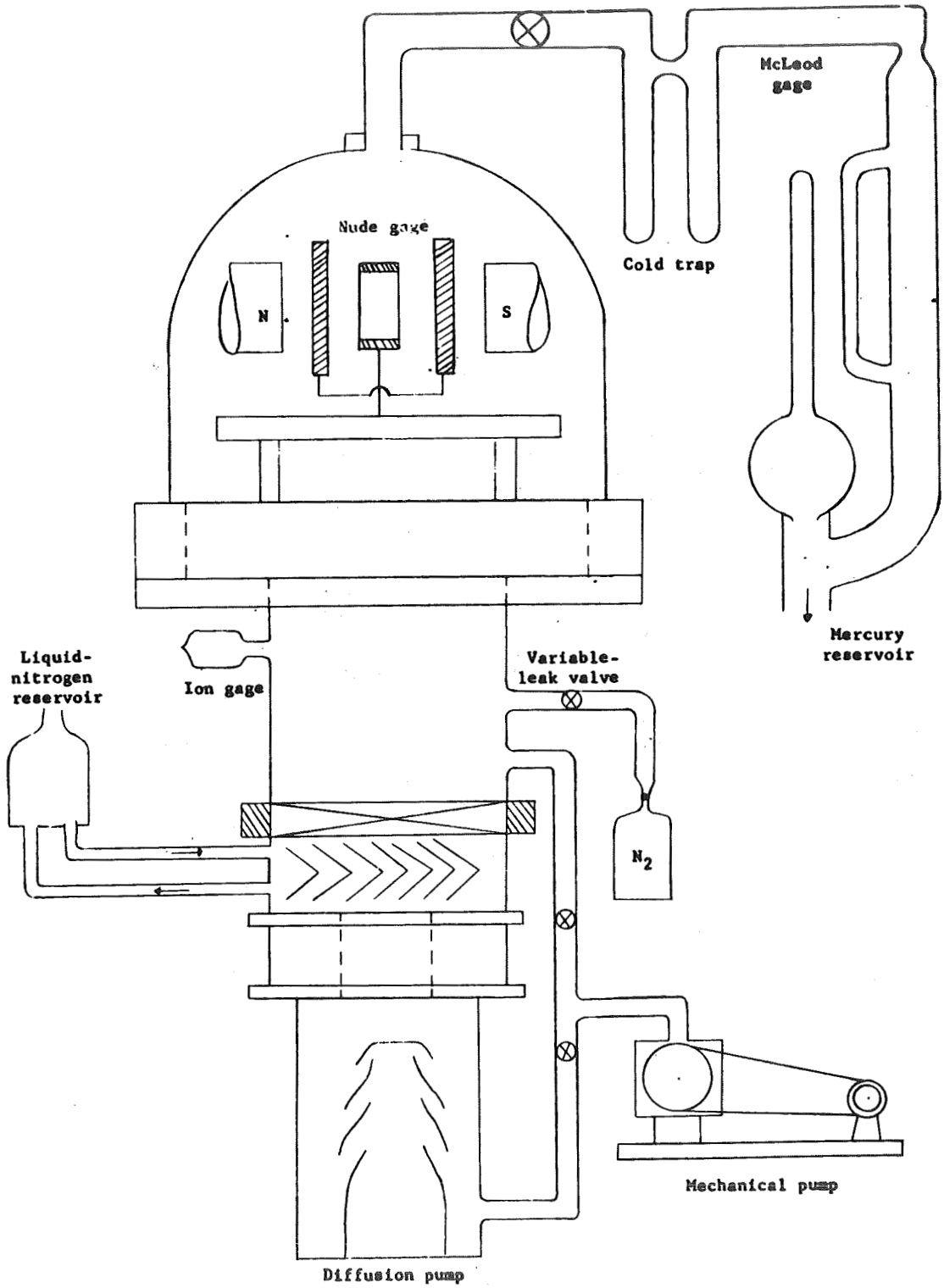


Figure 3.-Schematic drawing of test apparatus.

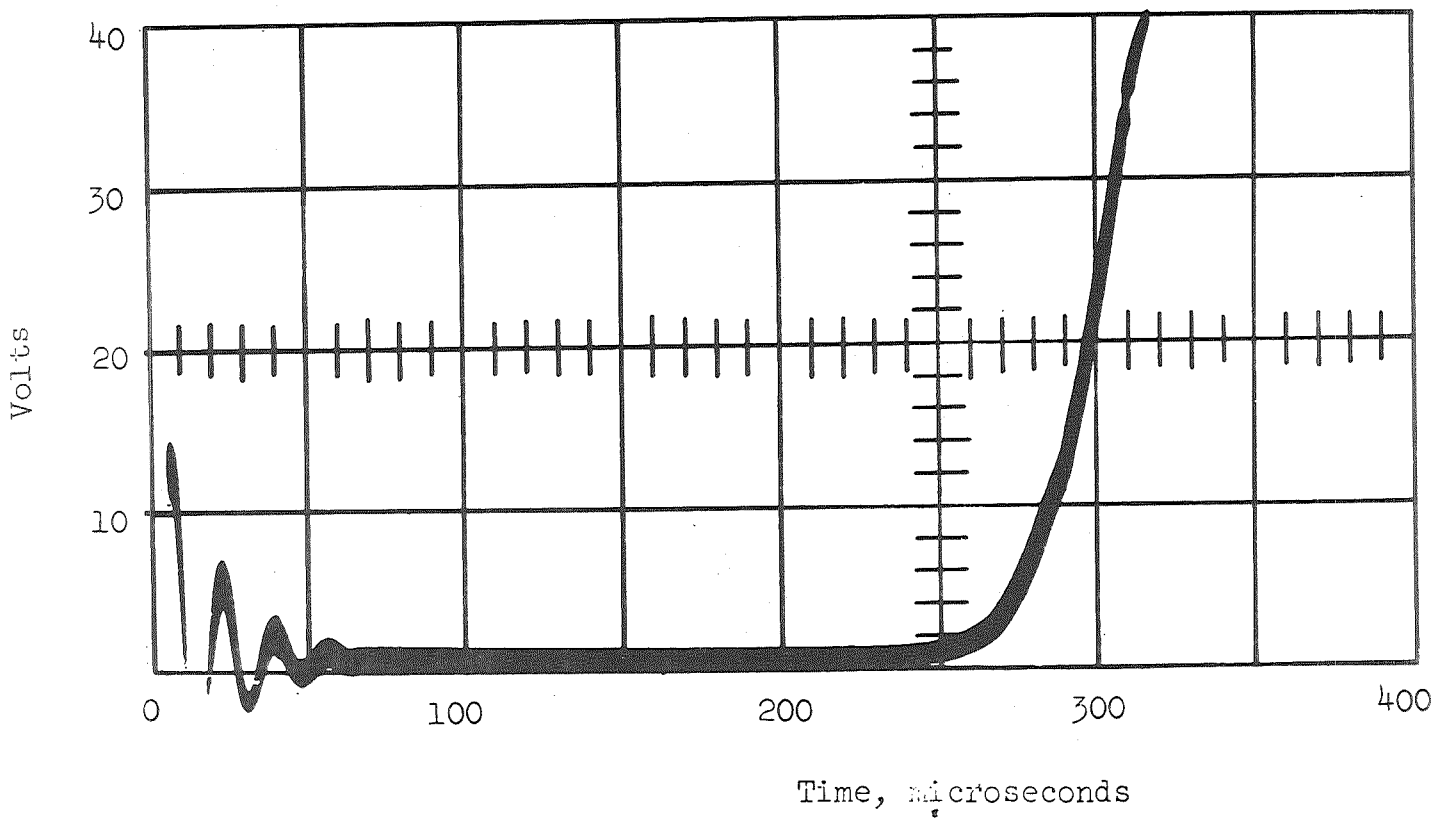


**Figure 4.-Typical record of time response measurement.**

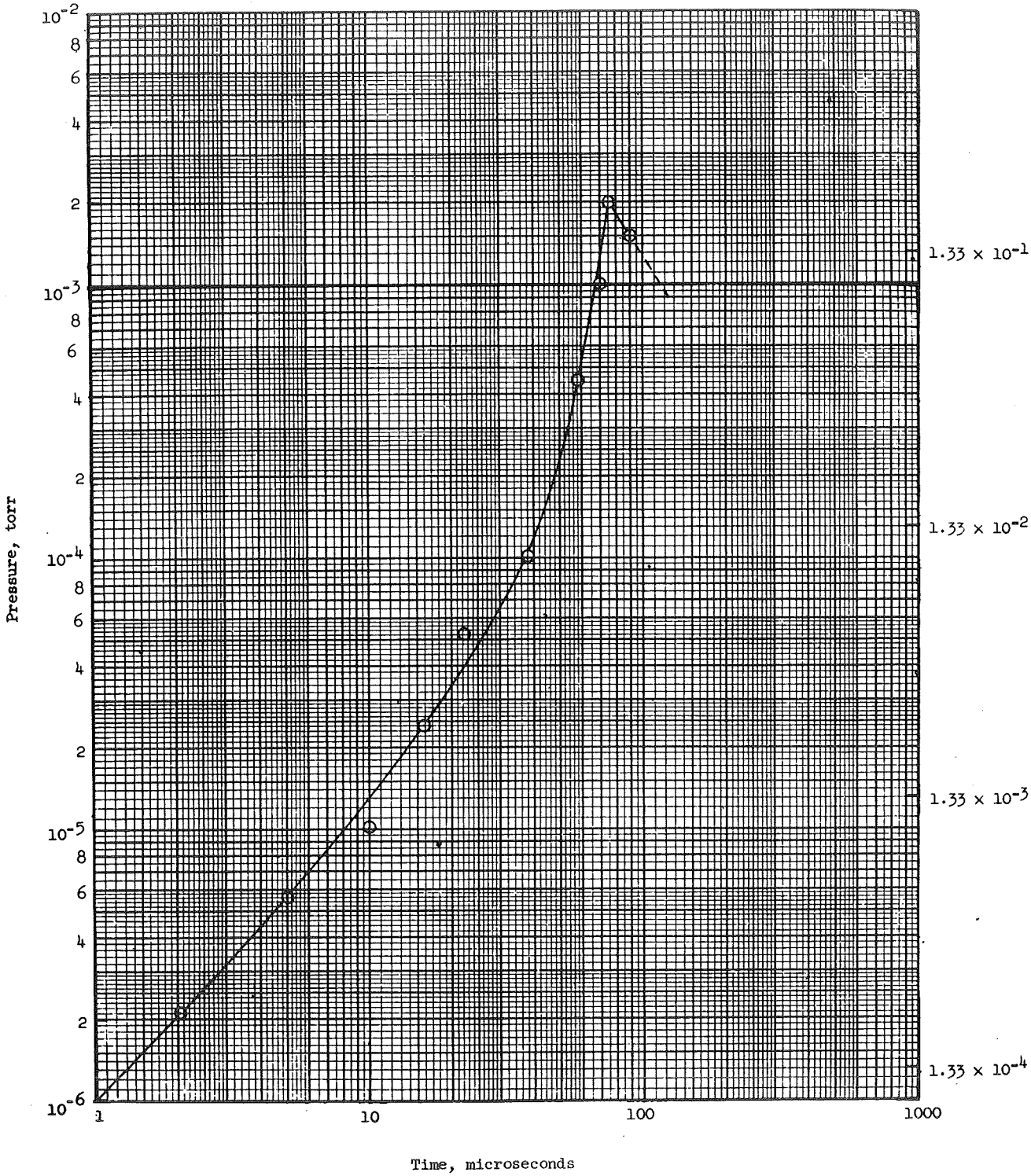


Figure 5.-Final configuration response-time curve.

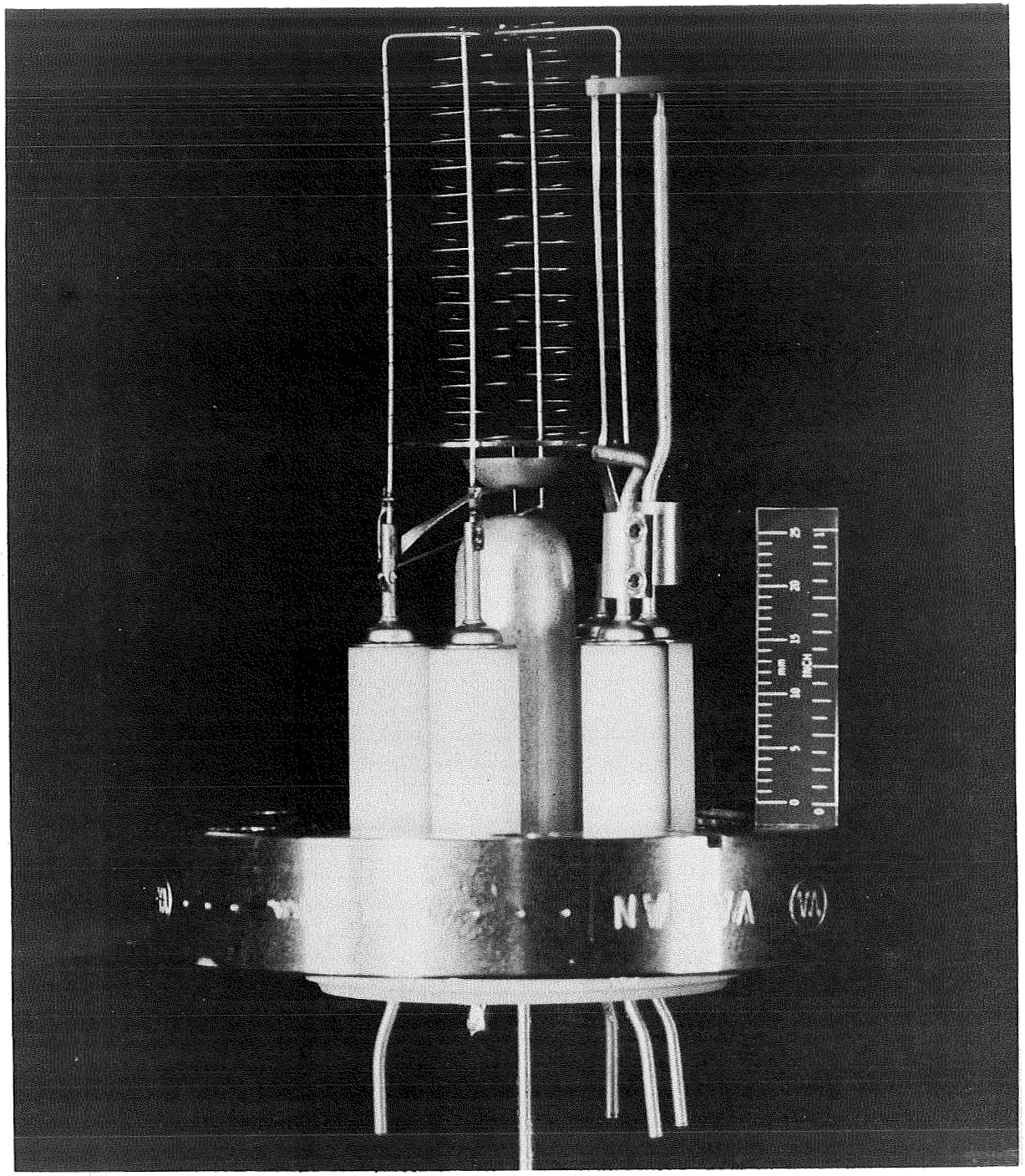

Figure 6.-Nude configuration of the buried collector (Melfi) gage.

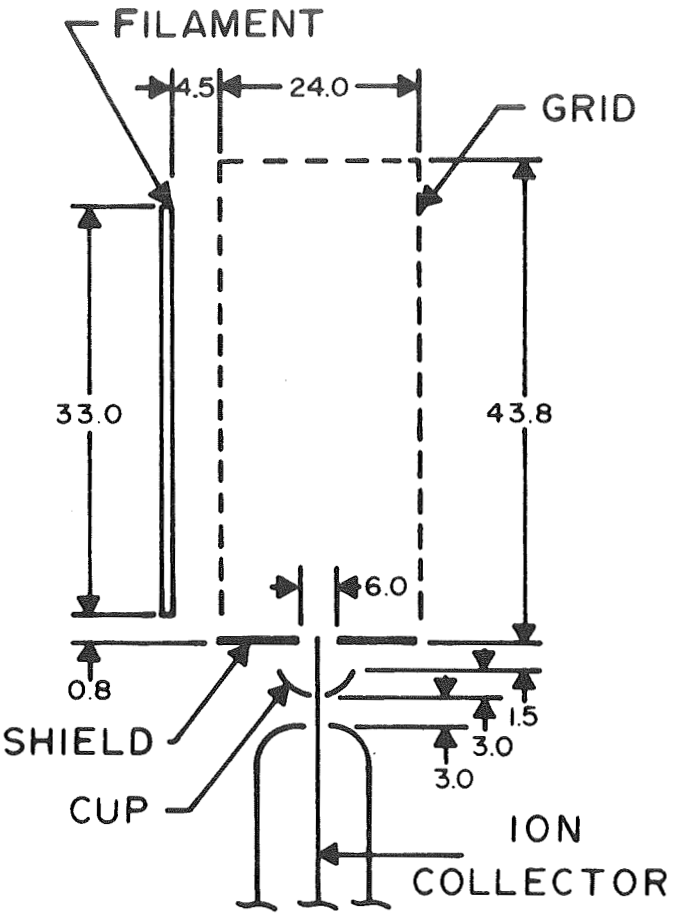


Figure 7.-Buried collector gage dimensional drawing. No scale.
Dimensions in millimeters.

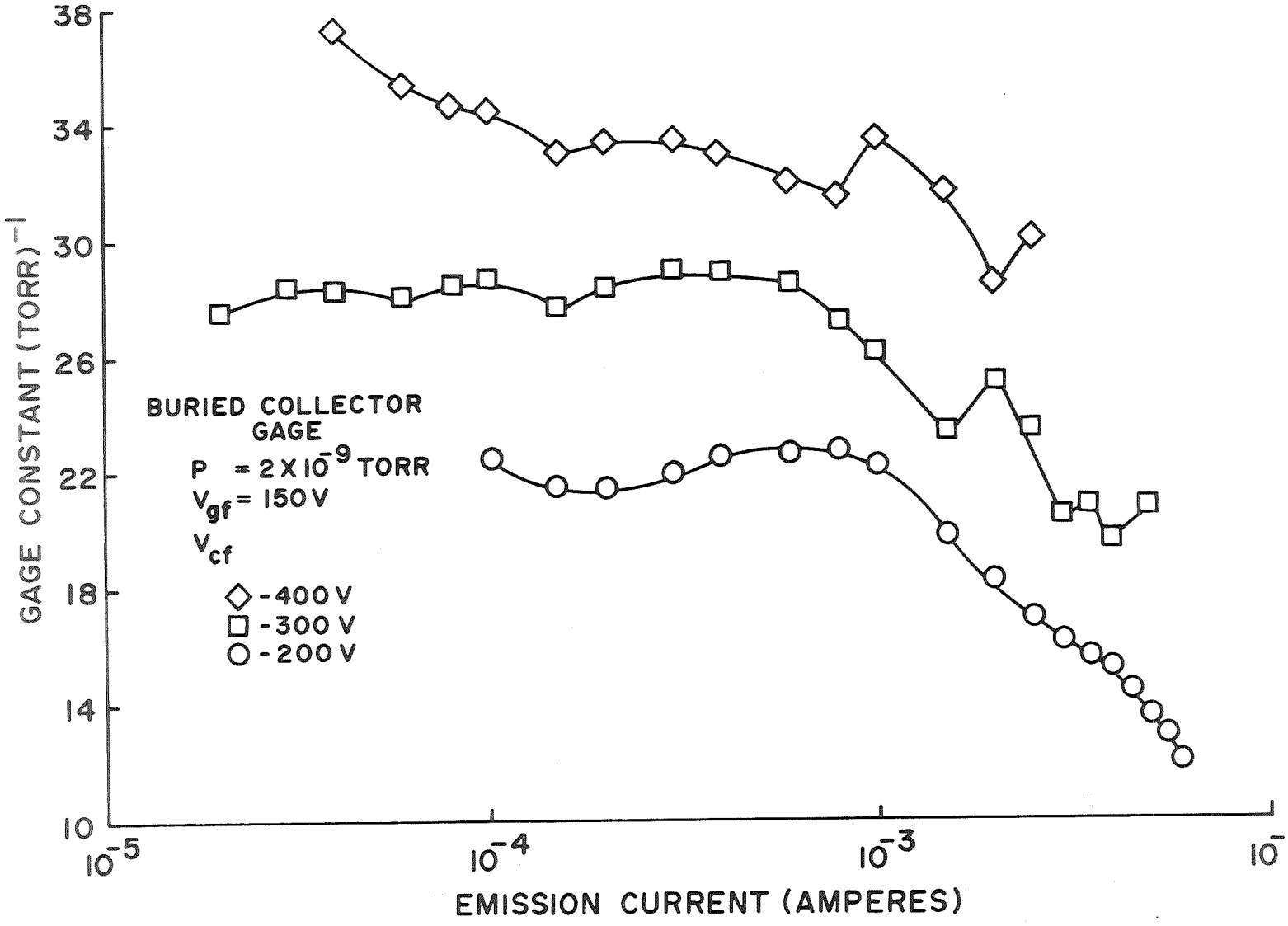


Figure 8.-Gage constant as a function of emission current for a number of collector to filament voltages ($V_{ef}$) for the buried collector gage.

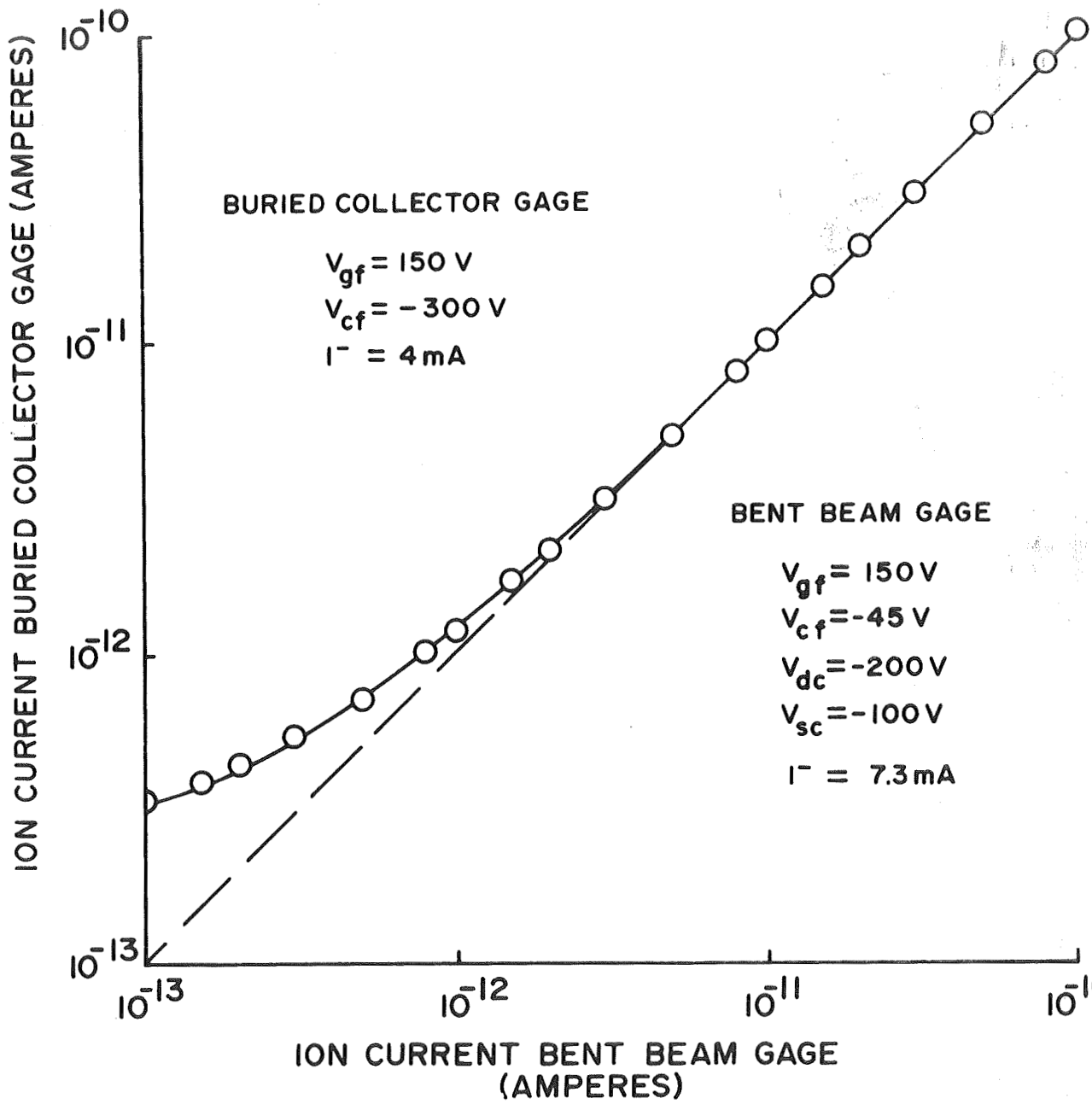


Figure 9.-X-ray background curve for the buried collector gage with the bent beam Helmer gage as the reference.

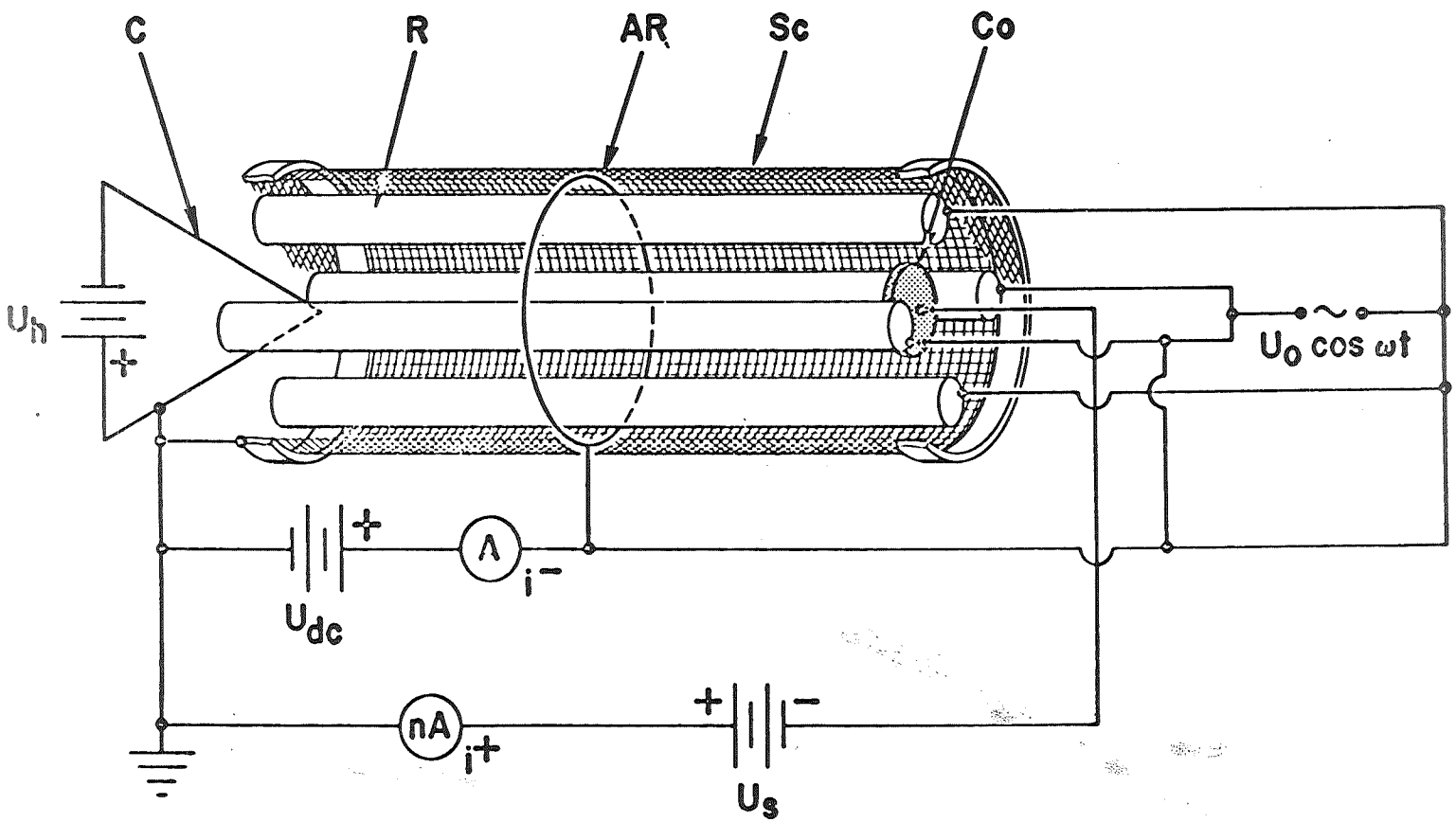


Figure 10.-Schematic drawing of the quadrupole ionization gage developed by Schwarz.

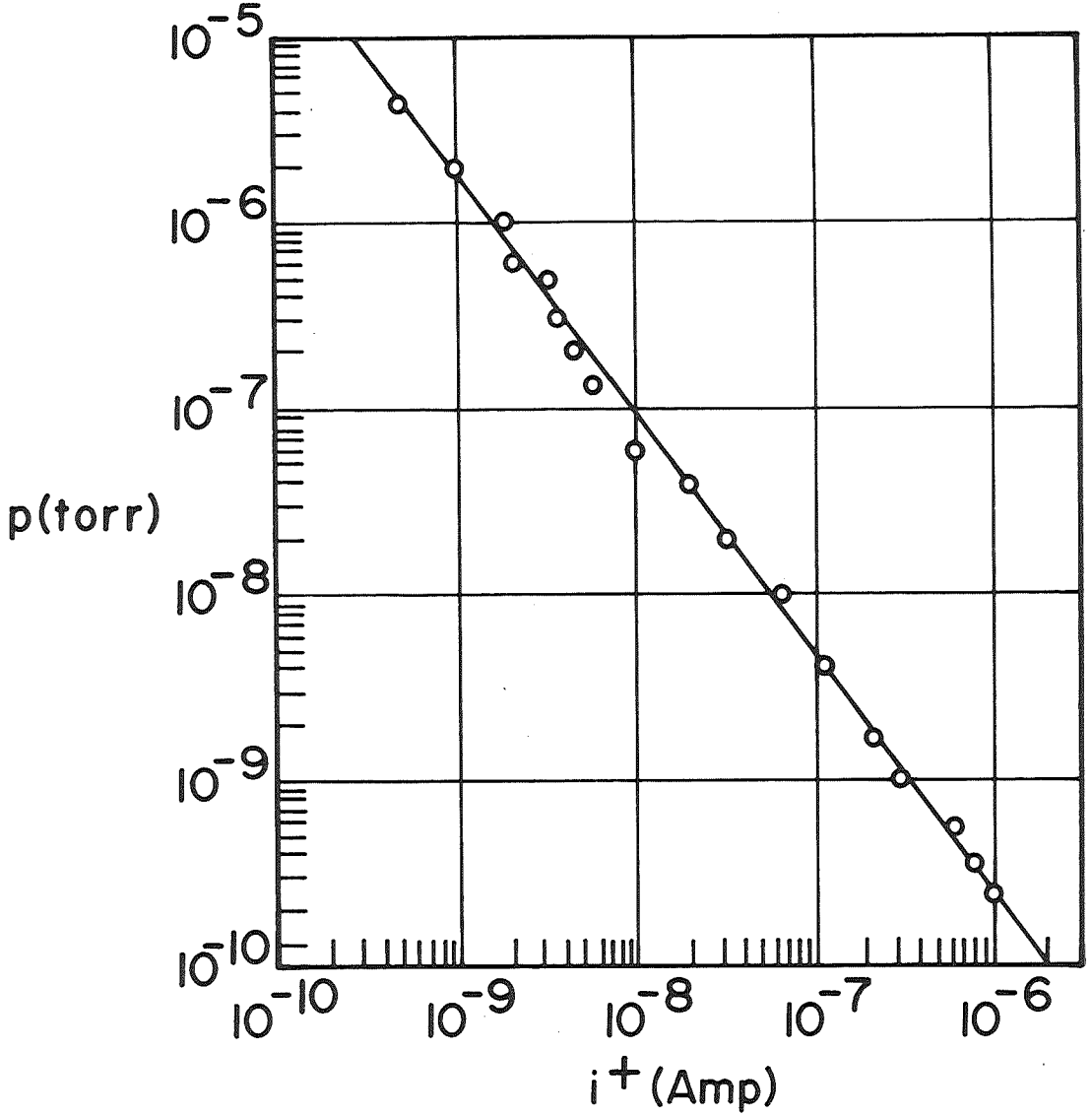


Figure 11.-Calibration curve of the quadrupole ionization gage with screen as ion collector at RF power of 20 watts.

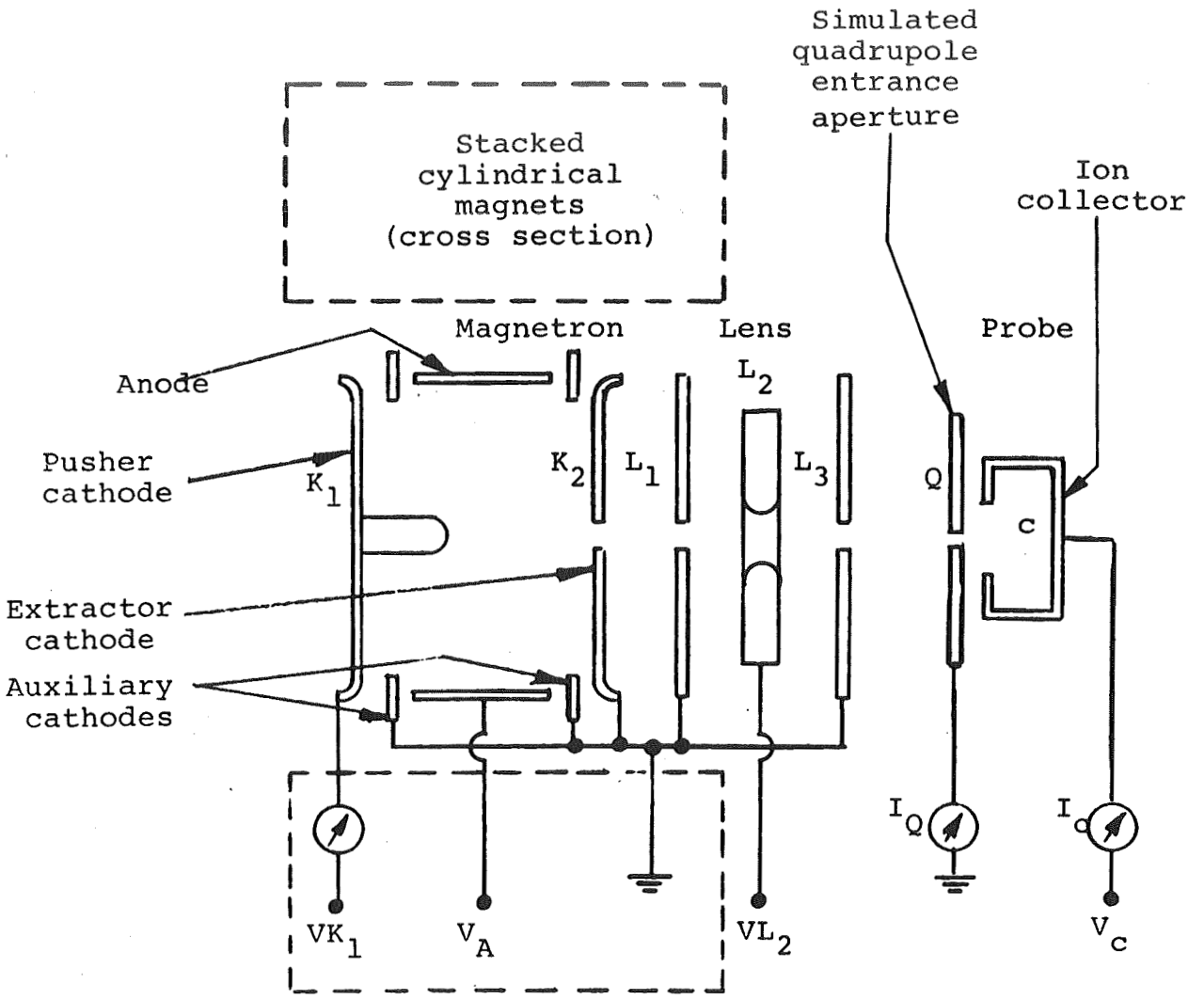


Figure 12.-Schematic drawing of cold-cathode ion source with lens.

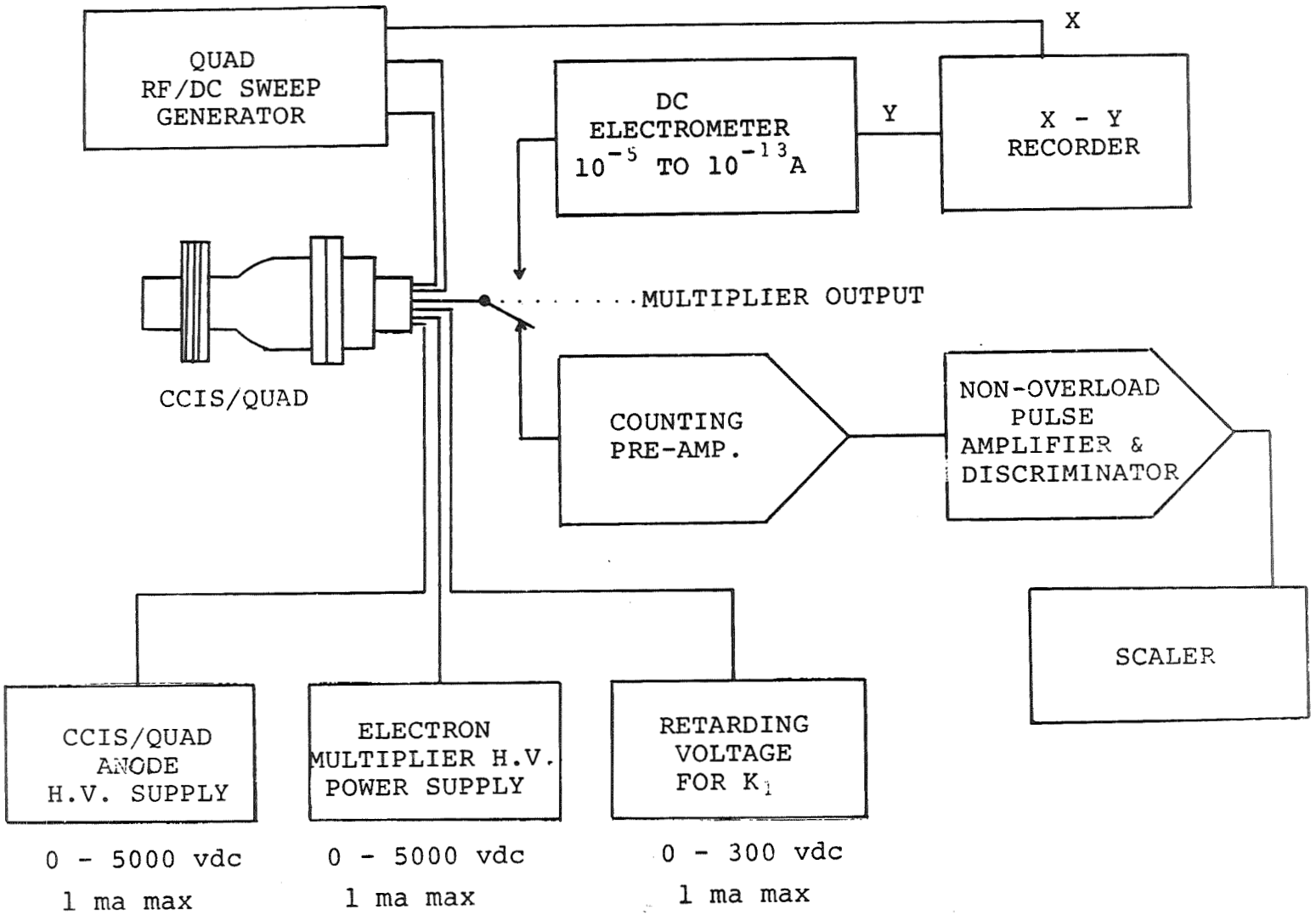


**Figure 13.-Block diagram of cold-cathode ion source/quadrupole experimental apparatus.**

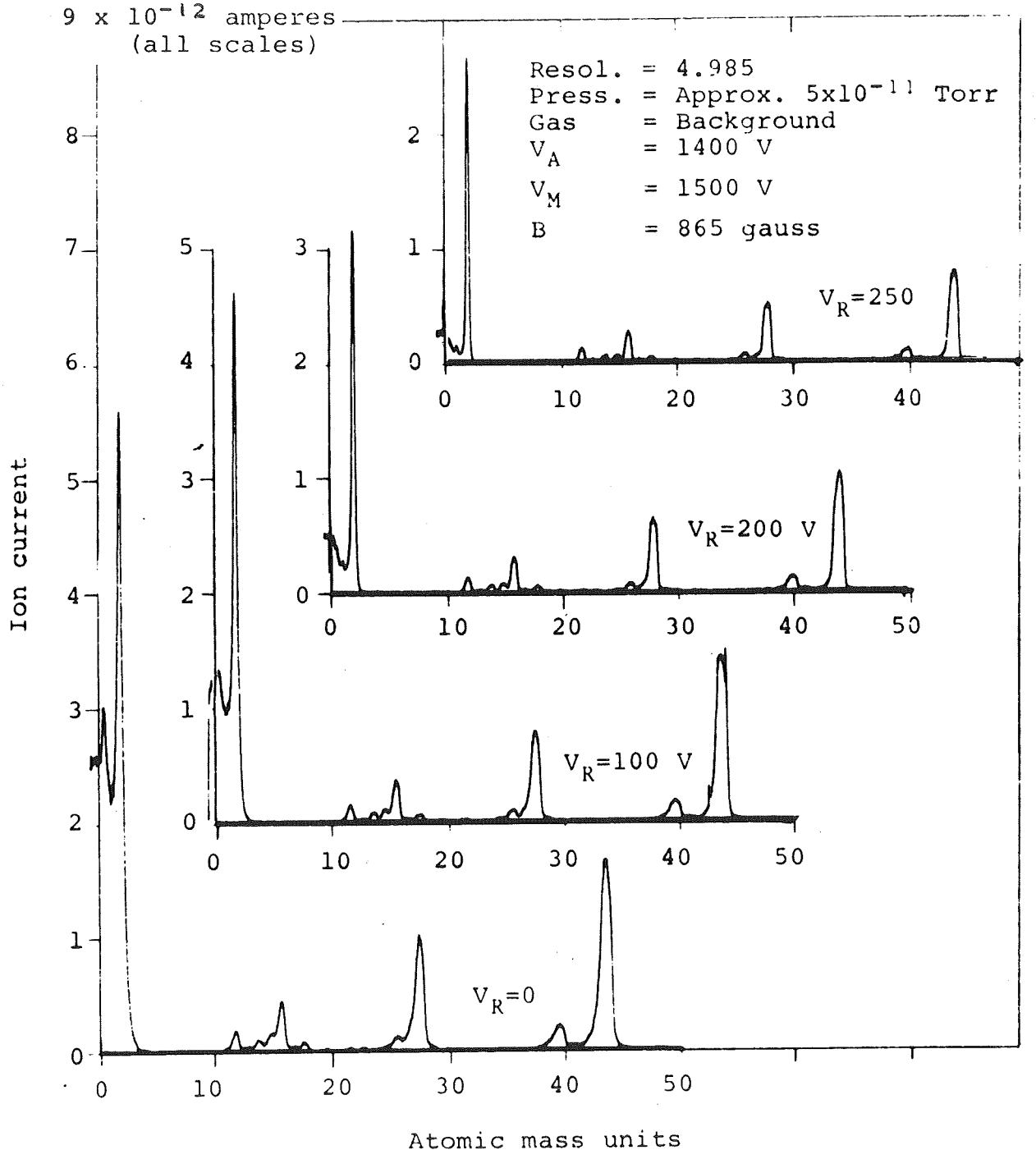


Figure 14.-CCIS/Quad DC signal and noise vs. retarding potential with tubular cathode stub.

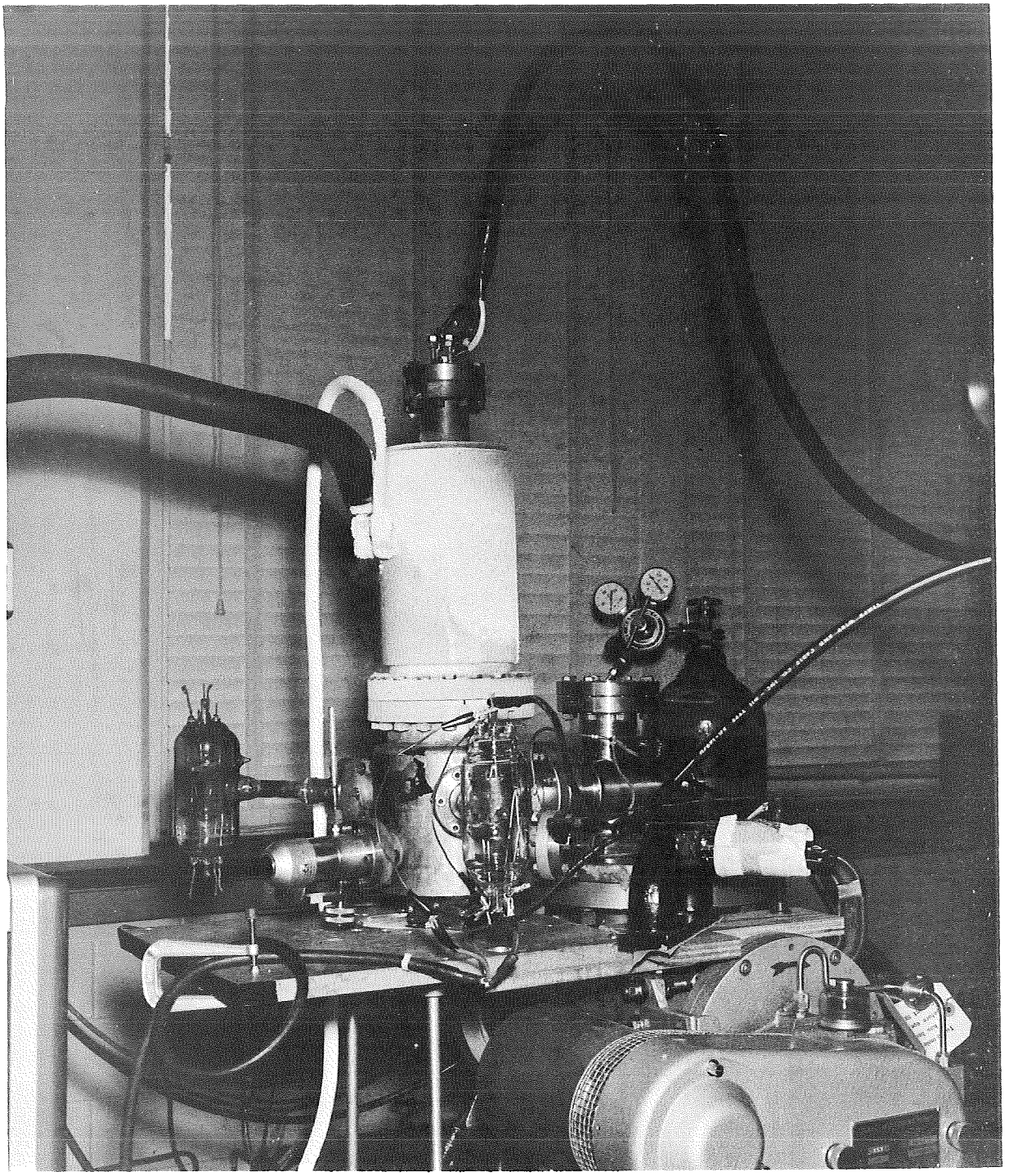

Figure 15.-Turbomolecular-titanium sublimation pumping system.

## Auxiliary Titanium Sublimation Pump

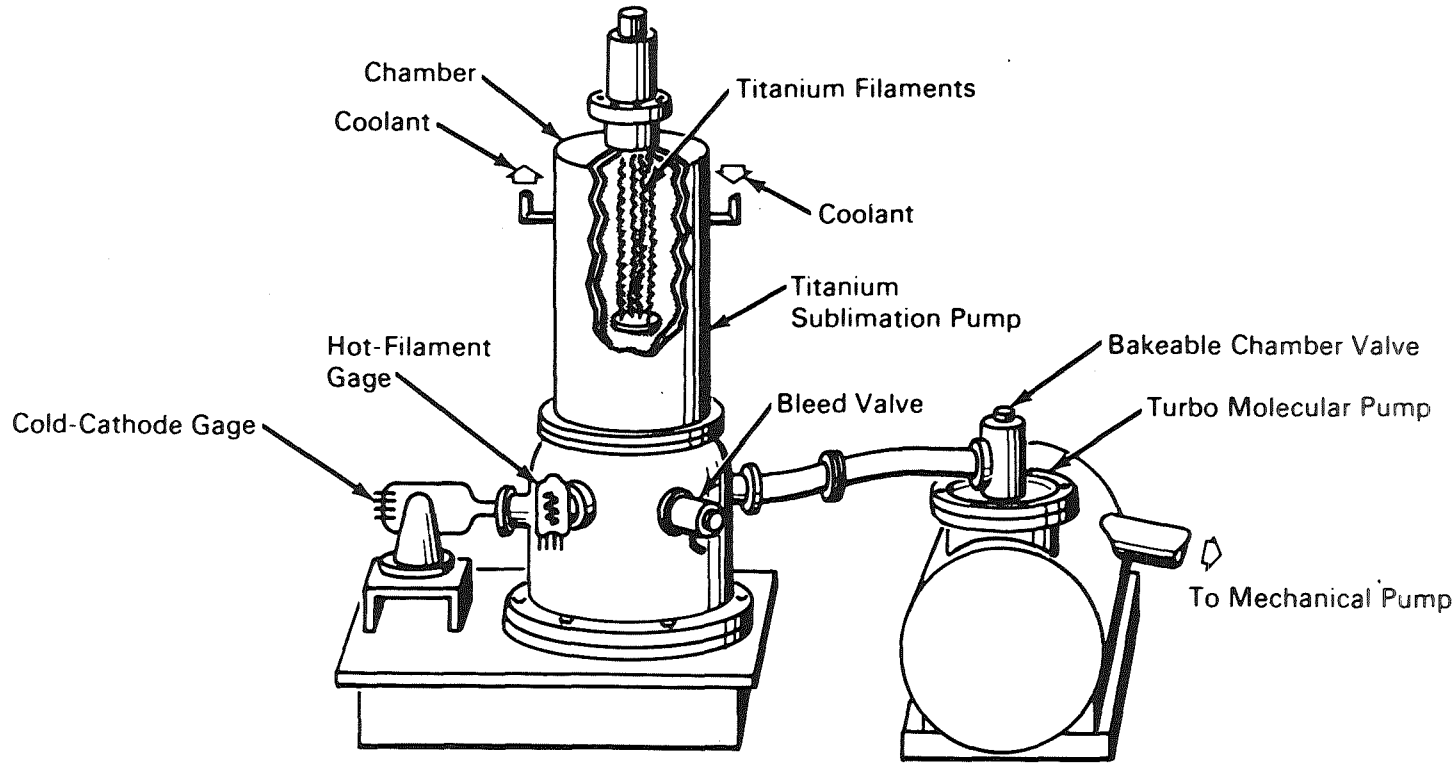


Figure 16.-Schematic drawing of turbomolecular-titanium sublimation system.

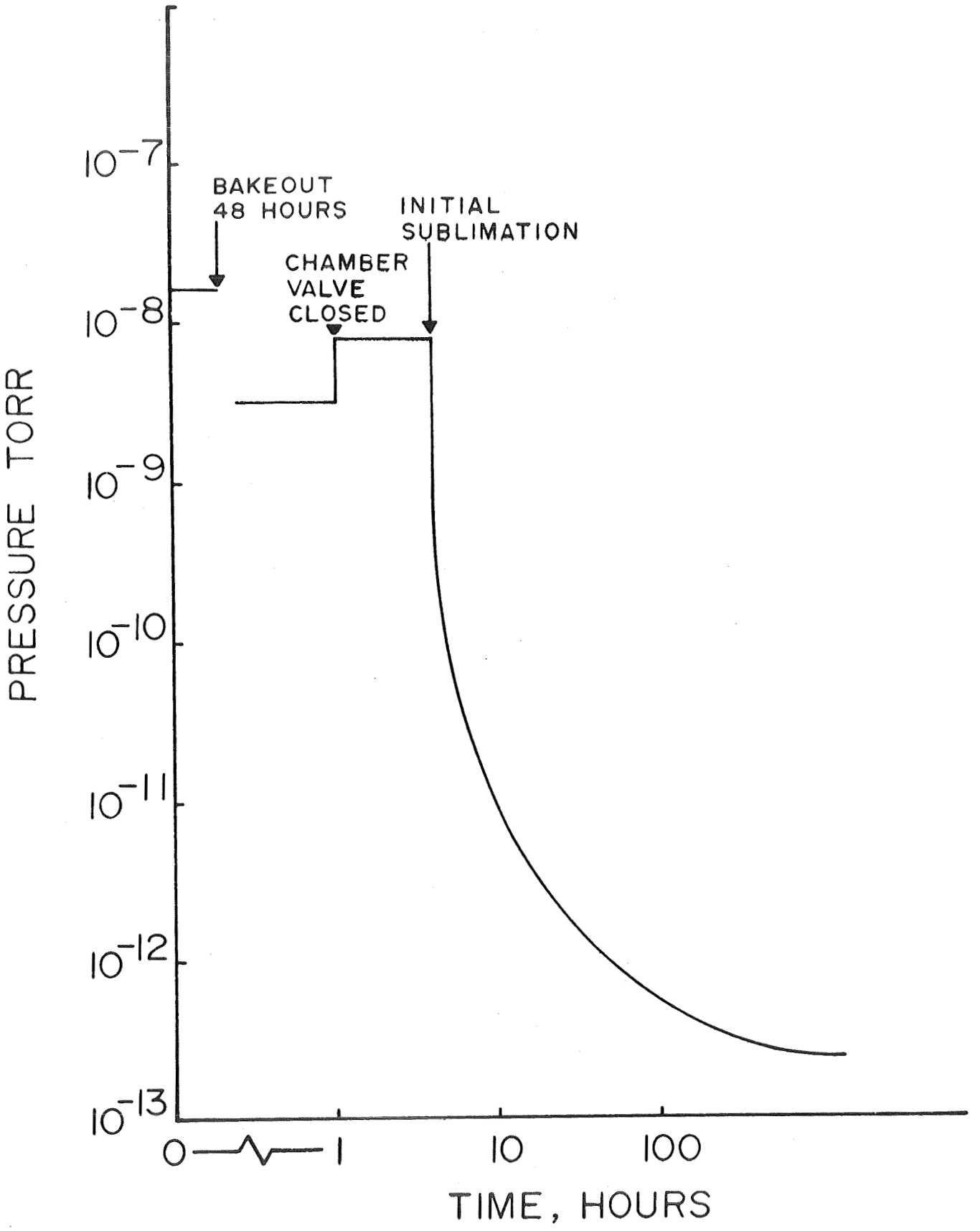


Figure 17.-Typical pump down curve for a turbomolecular-titanium sublimation pumping system.

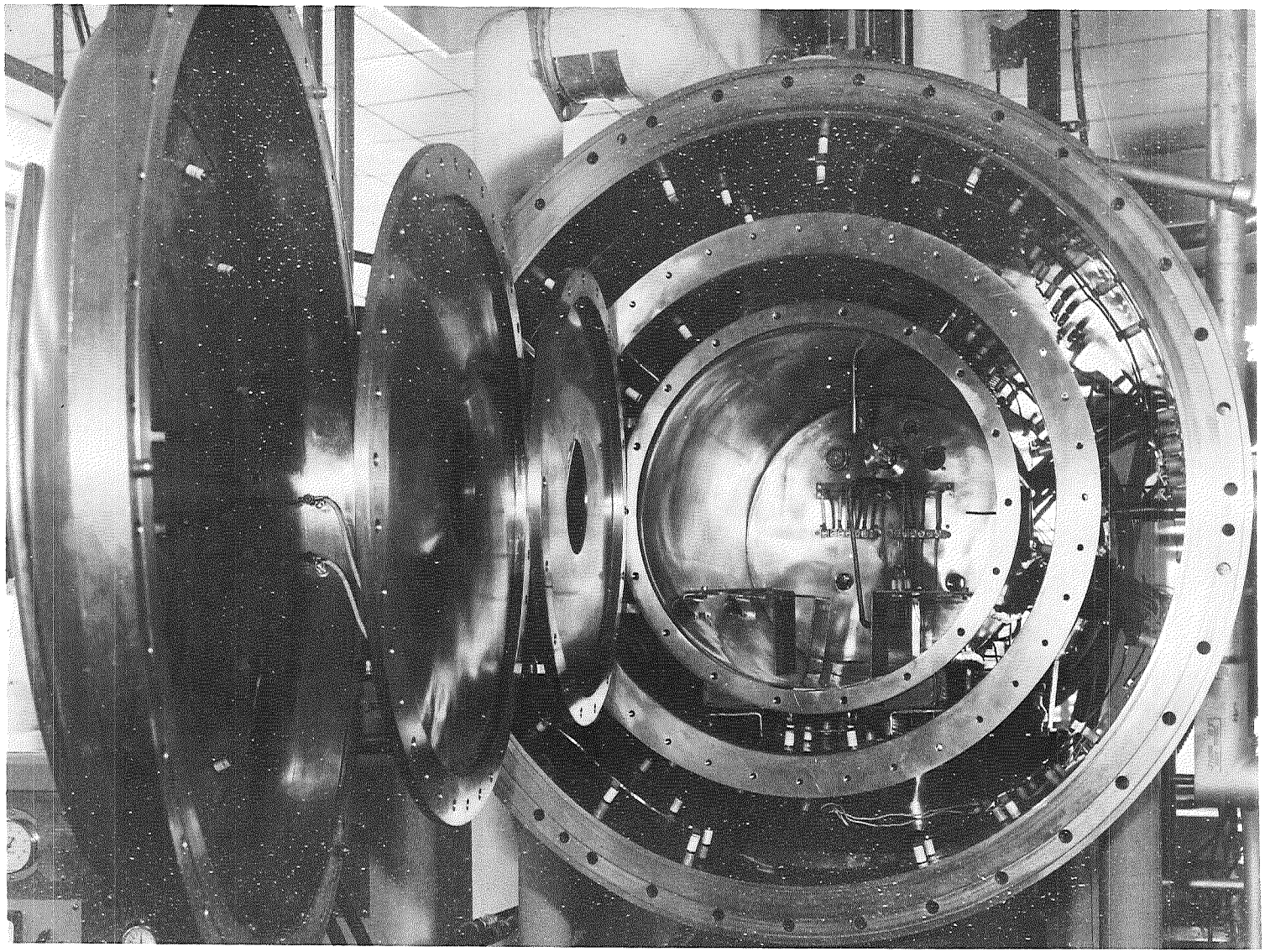

Figure 18.-XHV vacuum system showing the working chamber.

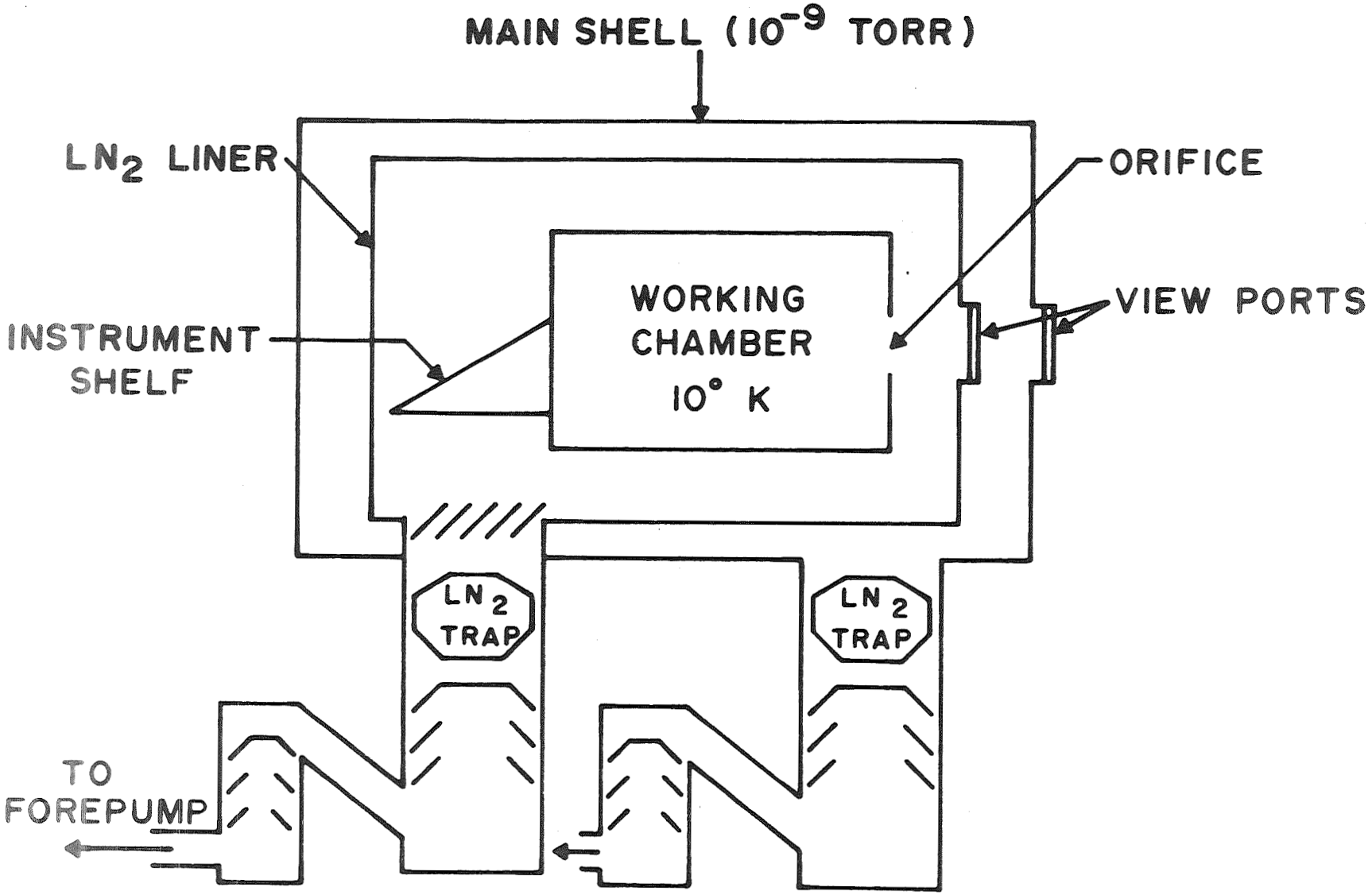


Figure 19.-Schematic drawing of the major components of the XHV vacuum system.

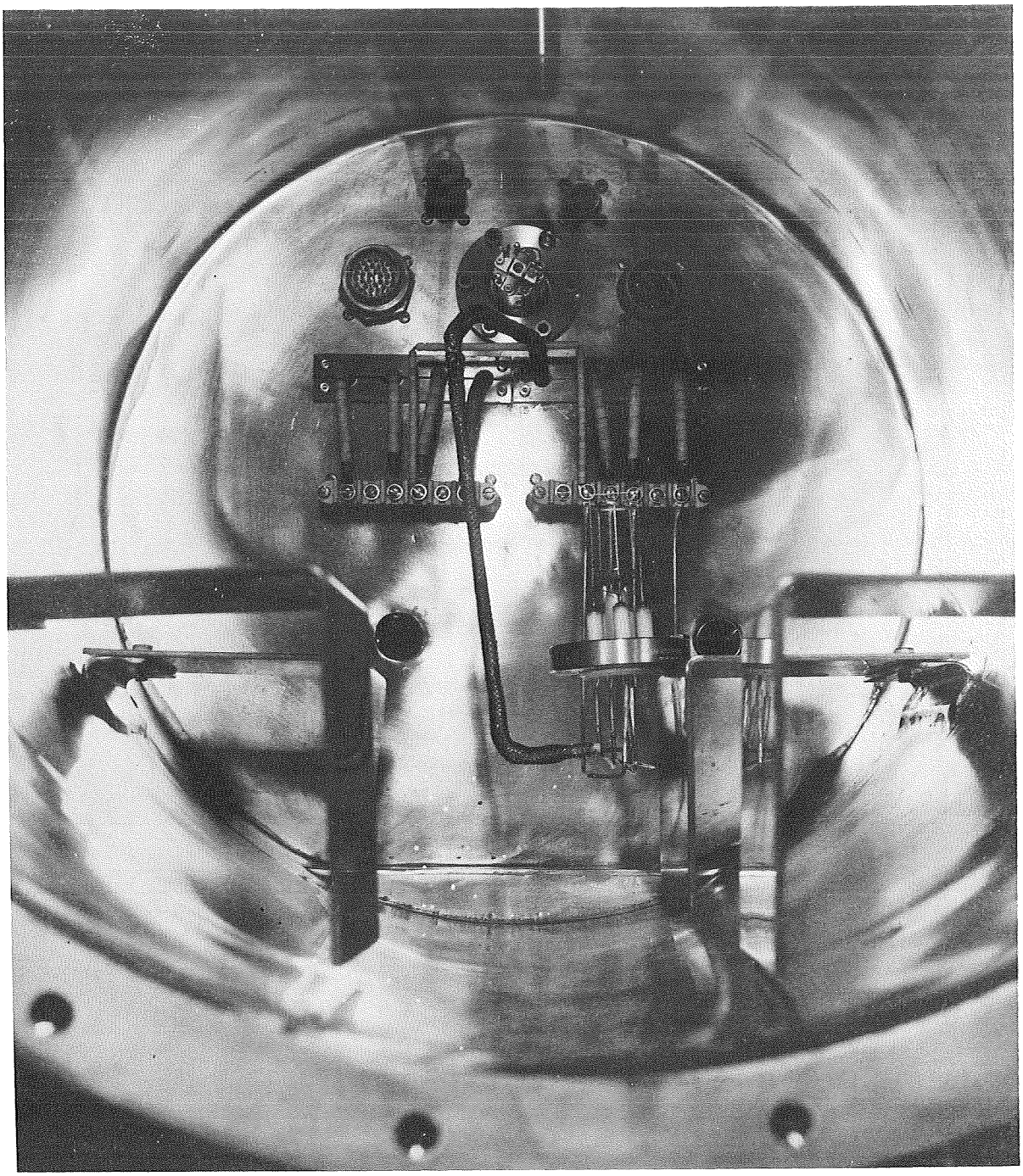

Figure 20.-Detail view of the XHV working chamber showing gage mounts, electrical feed-throughs, and quadrupole mounting.

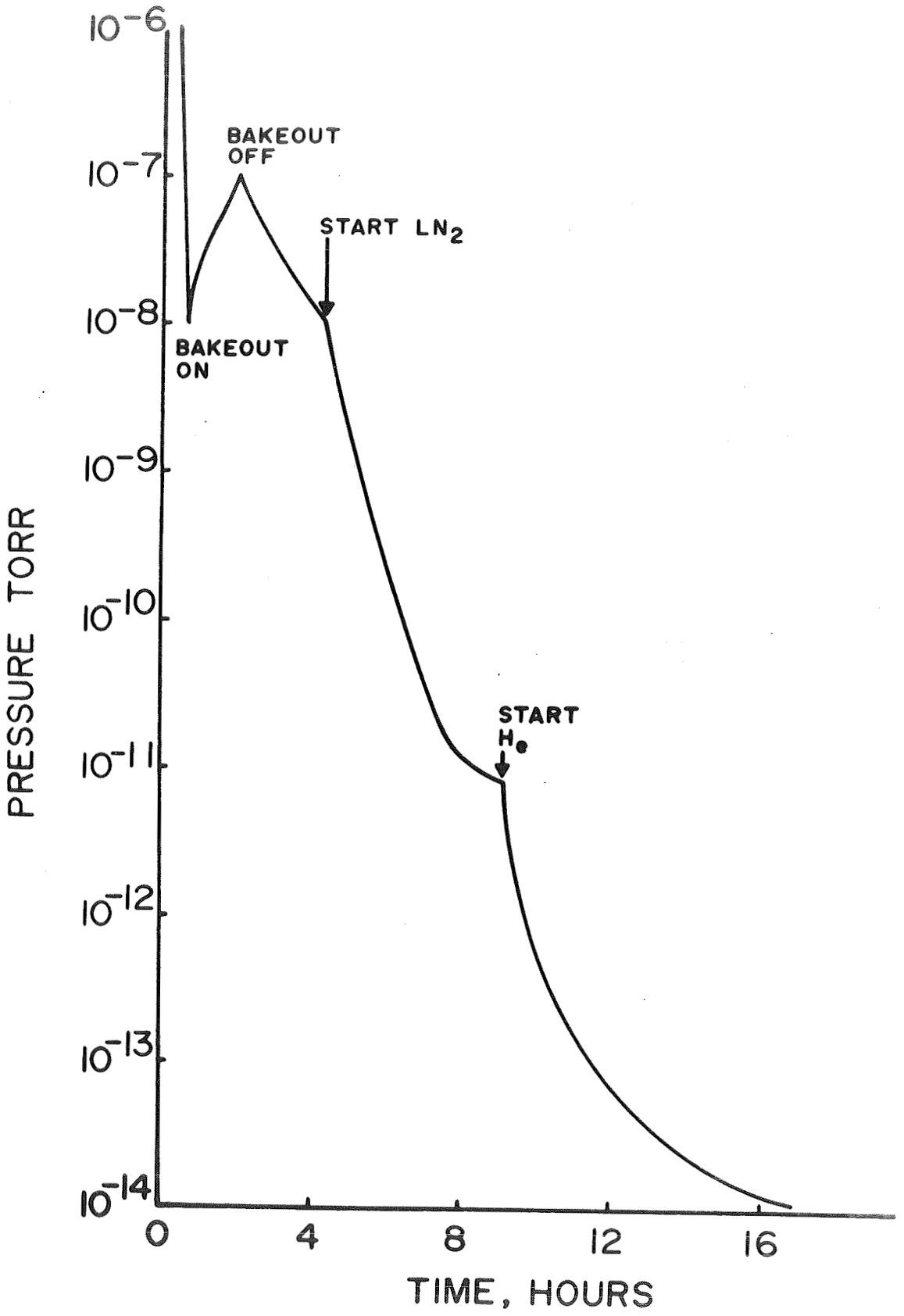


Figure 21.-Typical pump down curve for the XHV vacuum system.

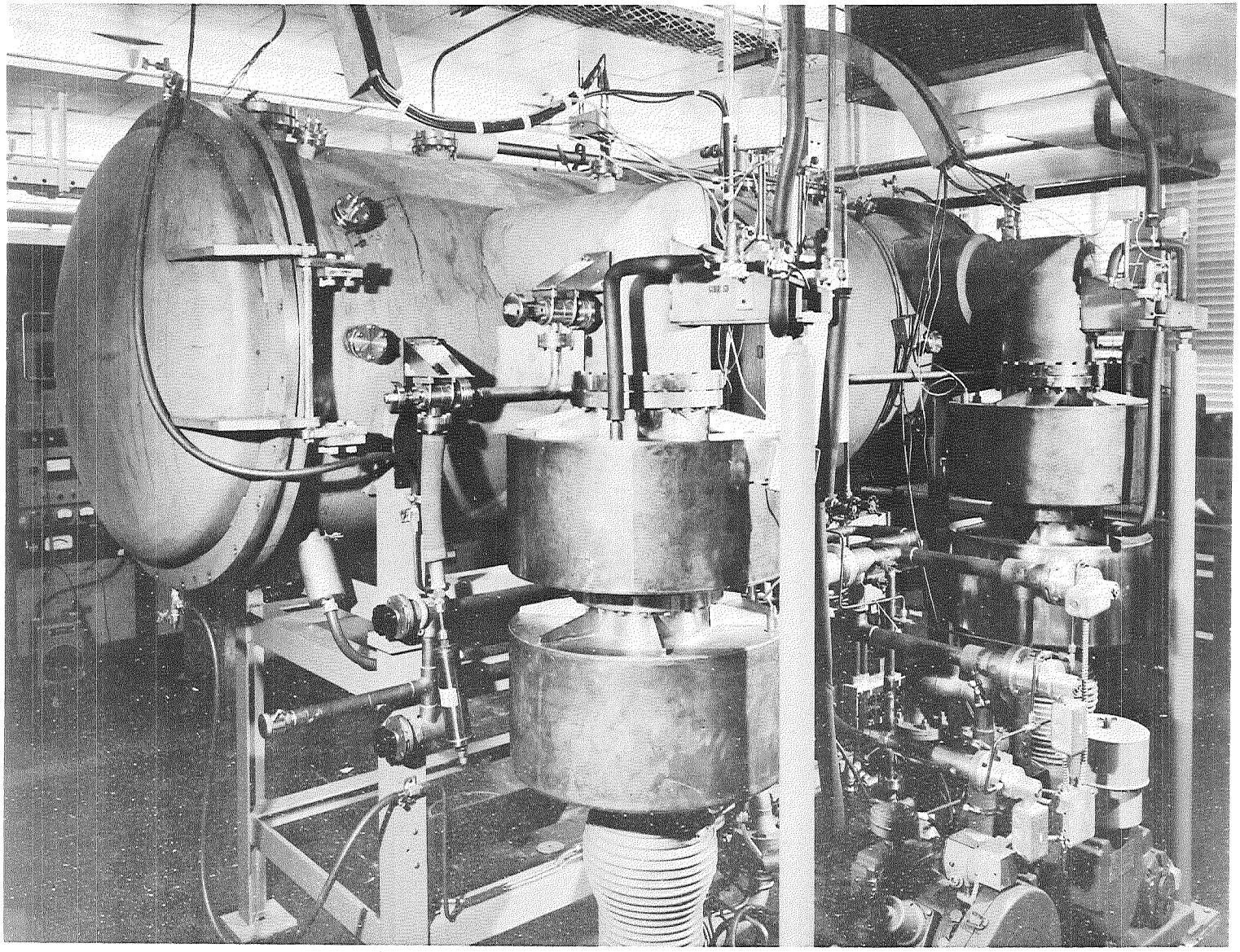

Figure 22.-Molecular beam system used for vacuum gage calibration and development.

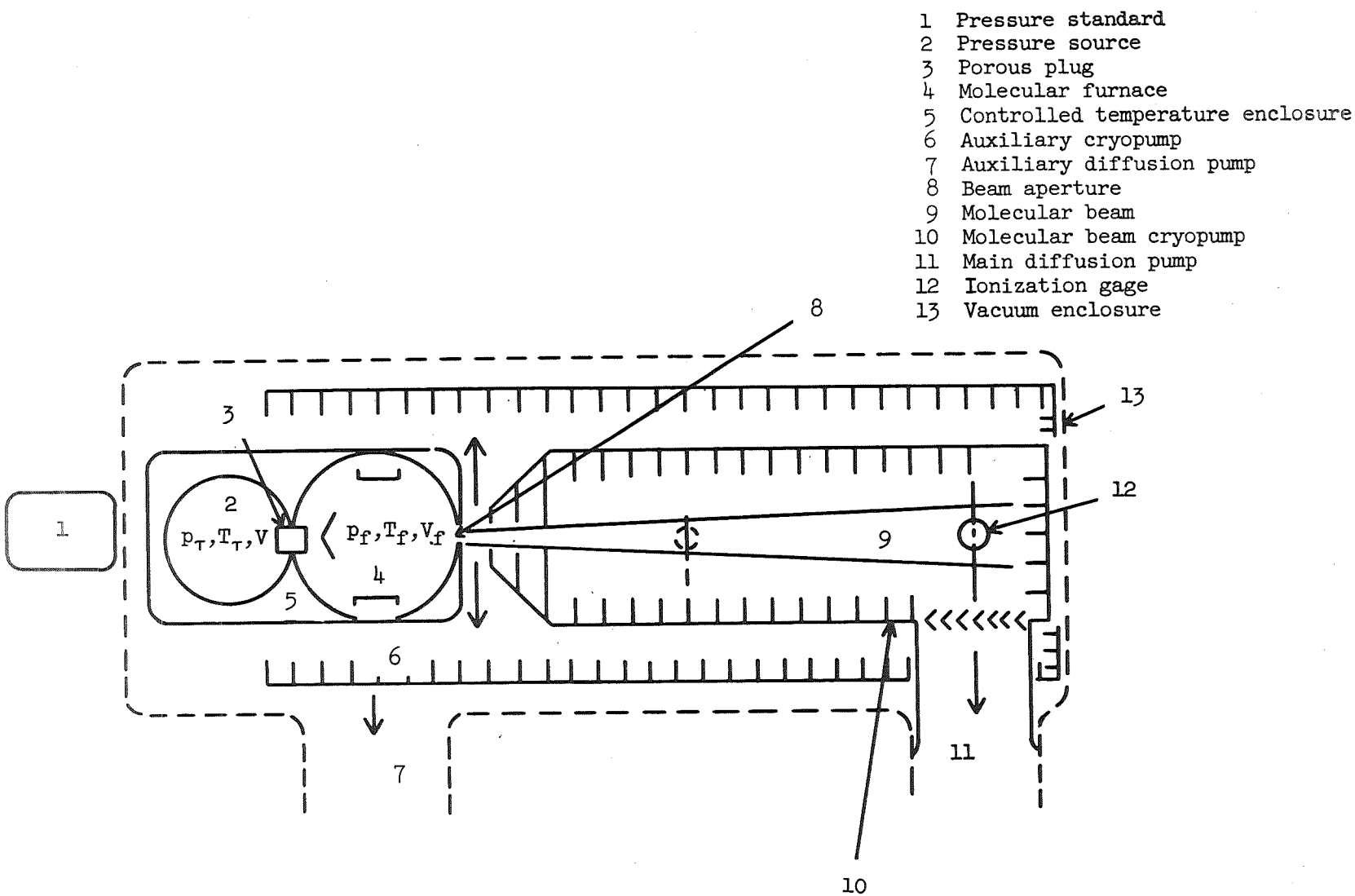


Figure 23.-Schematic drawing of major components of the molecular beam vacuum system.

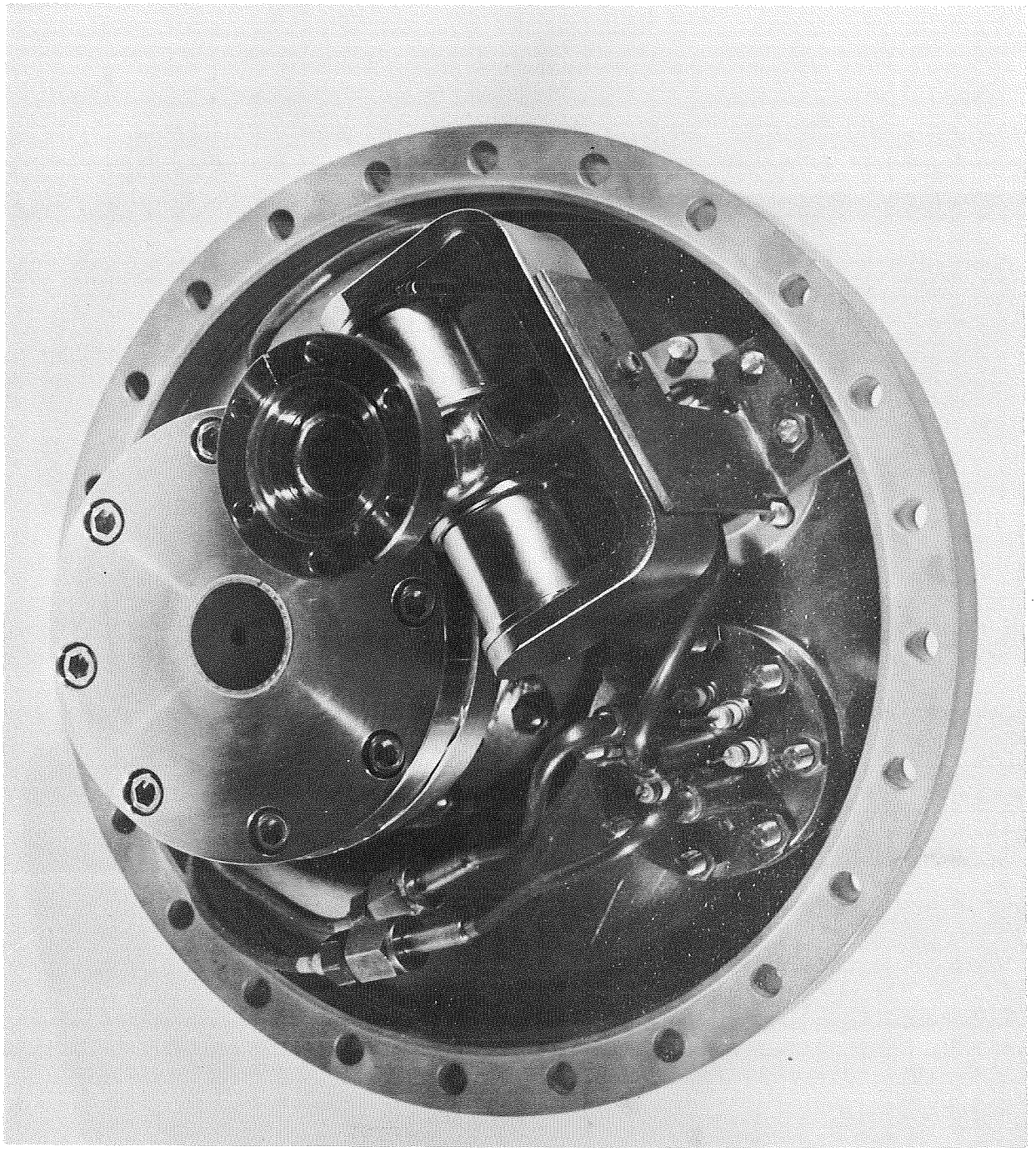

Figure 24.-Furnace section of the molecular beam system showing furnace orifice and gage for background pressure measurement.

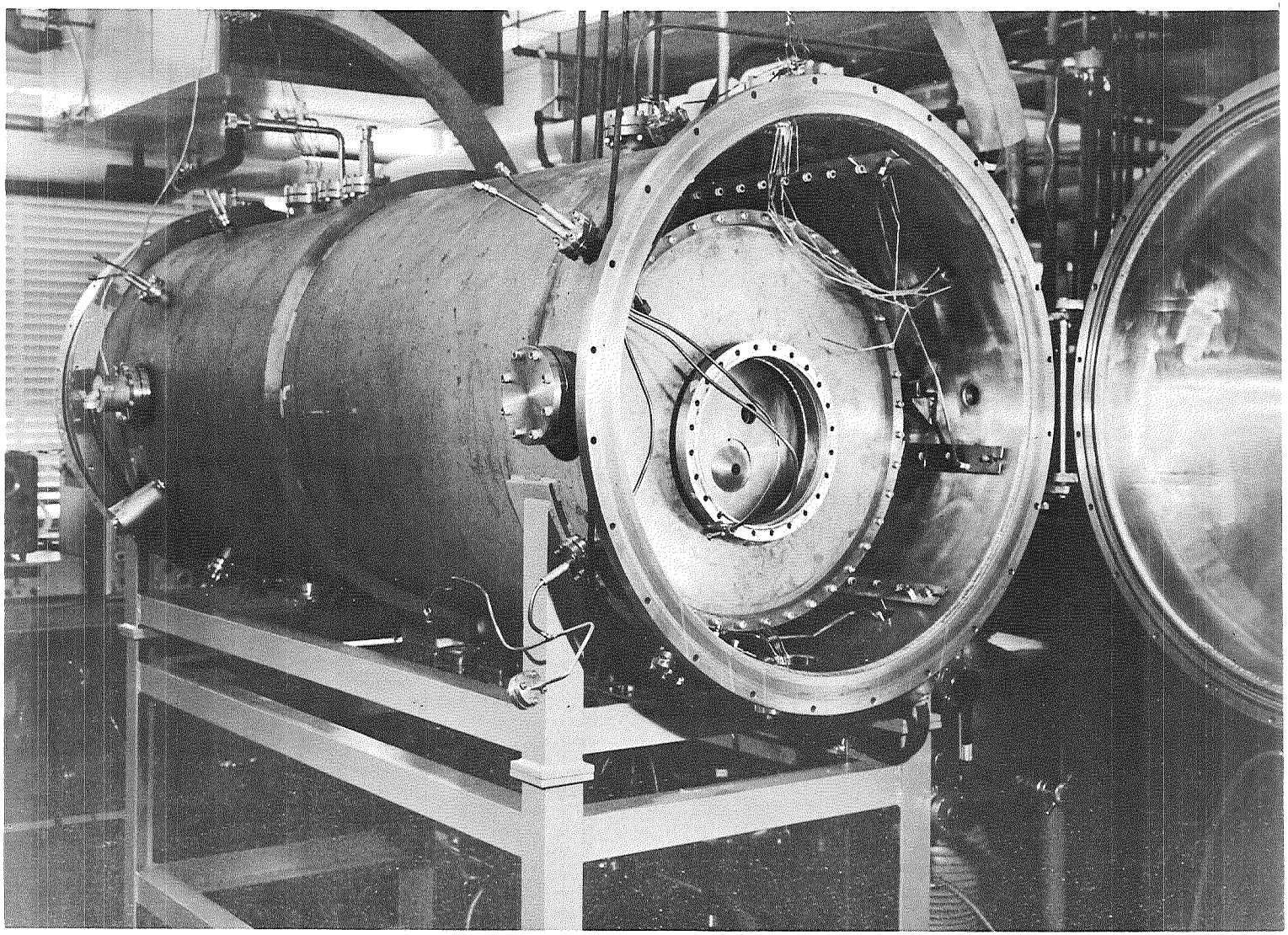

Figure 25.-Interior of molecular beam system showing furnace mounting ring, gage port, and LHe stripper.

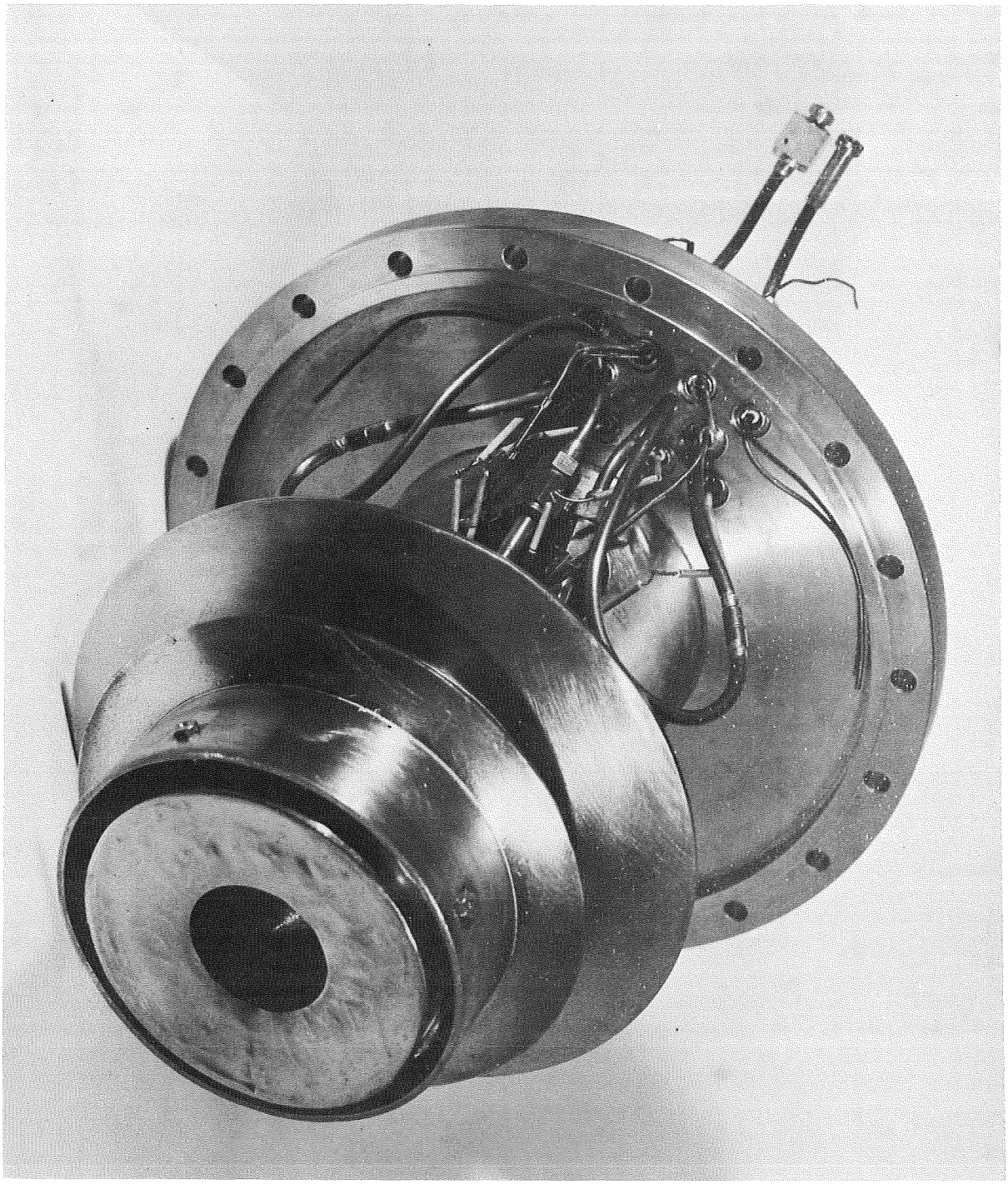

Figure 26.-Molecule beam test gage enclosure (thermal equilibrium chamber) showing beam entrance port and baffle.

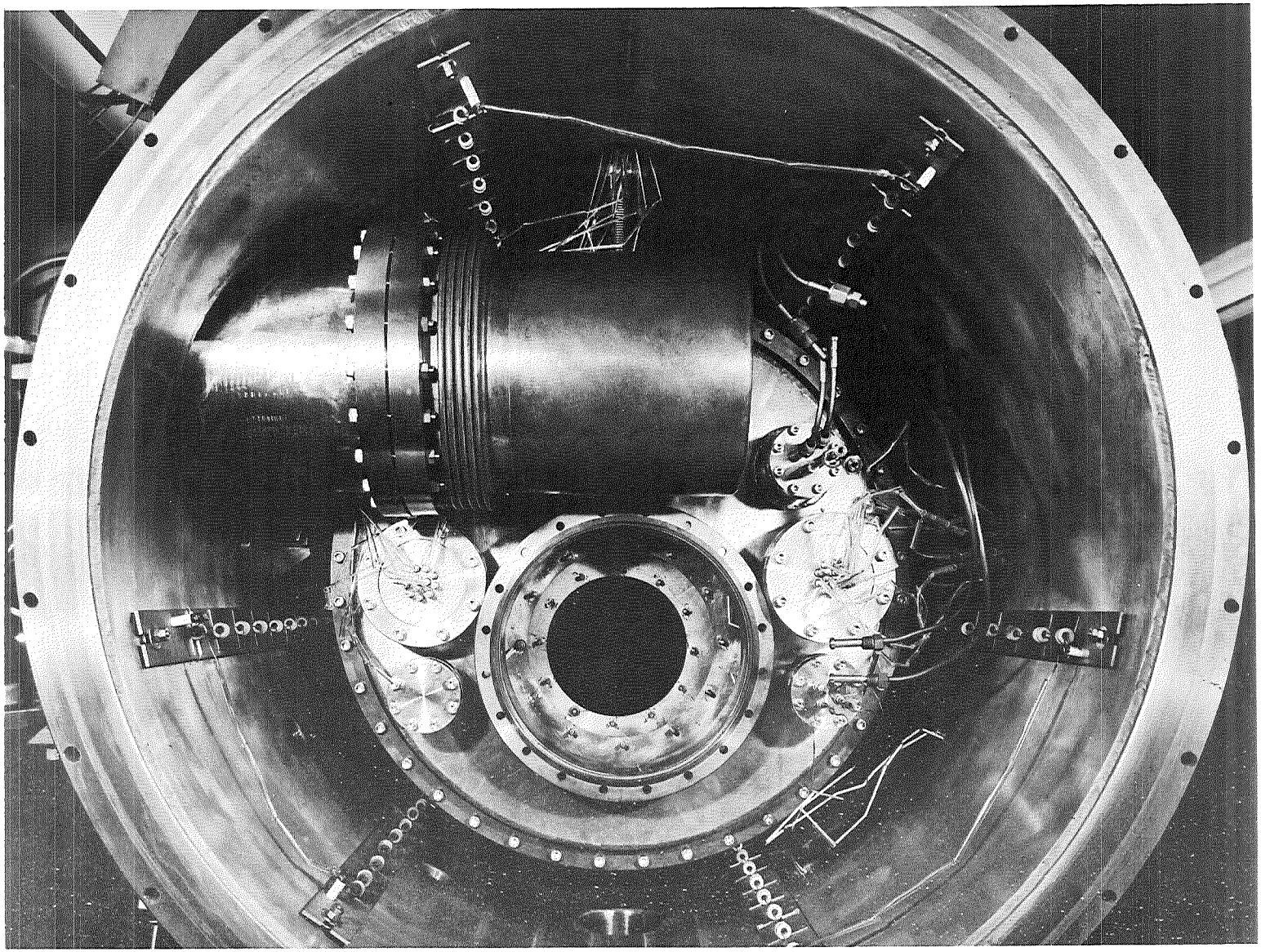

Figure 27.-Interior of molecular beam system showing gage enclosure mounting.

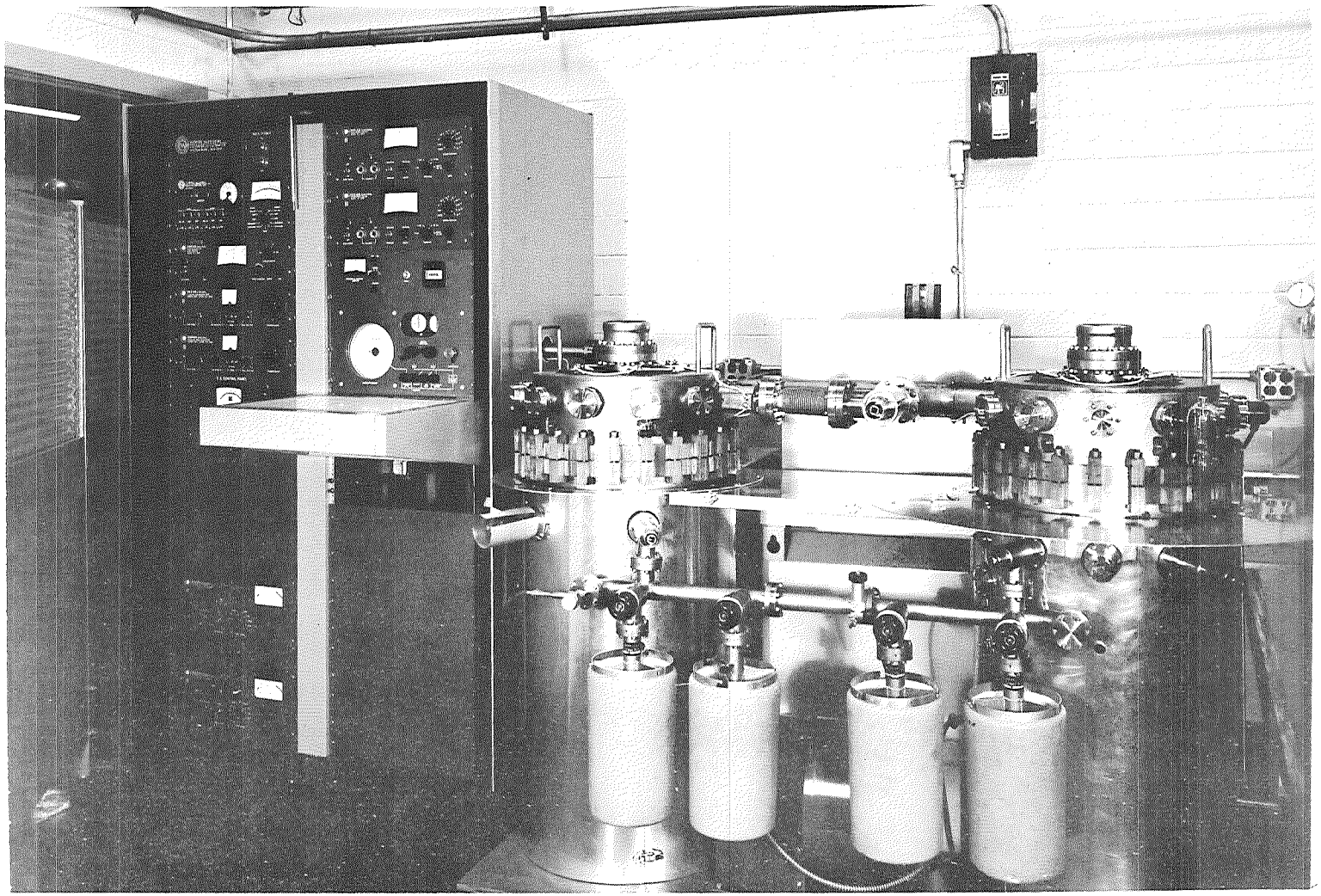

Figure 28.- Standard vacuum gage calibration system used as primary reference at LRC.

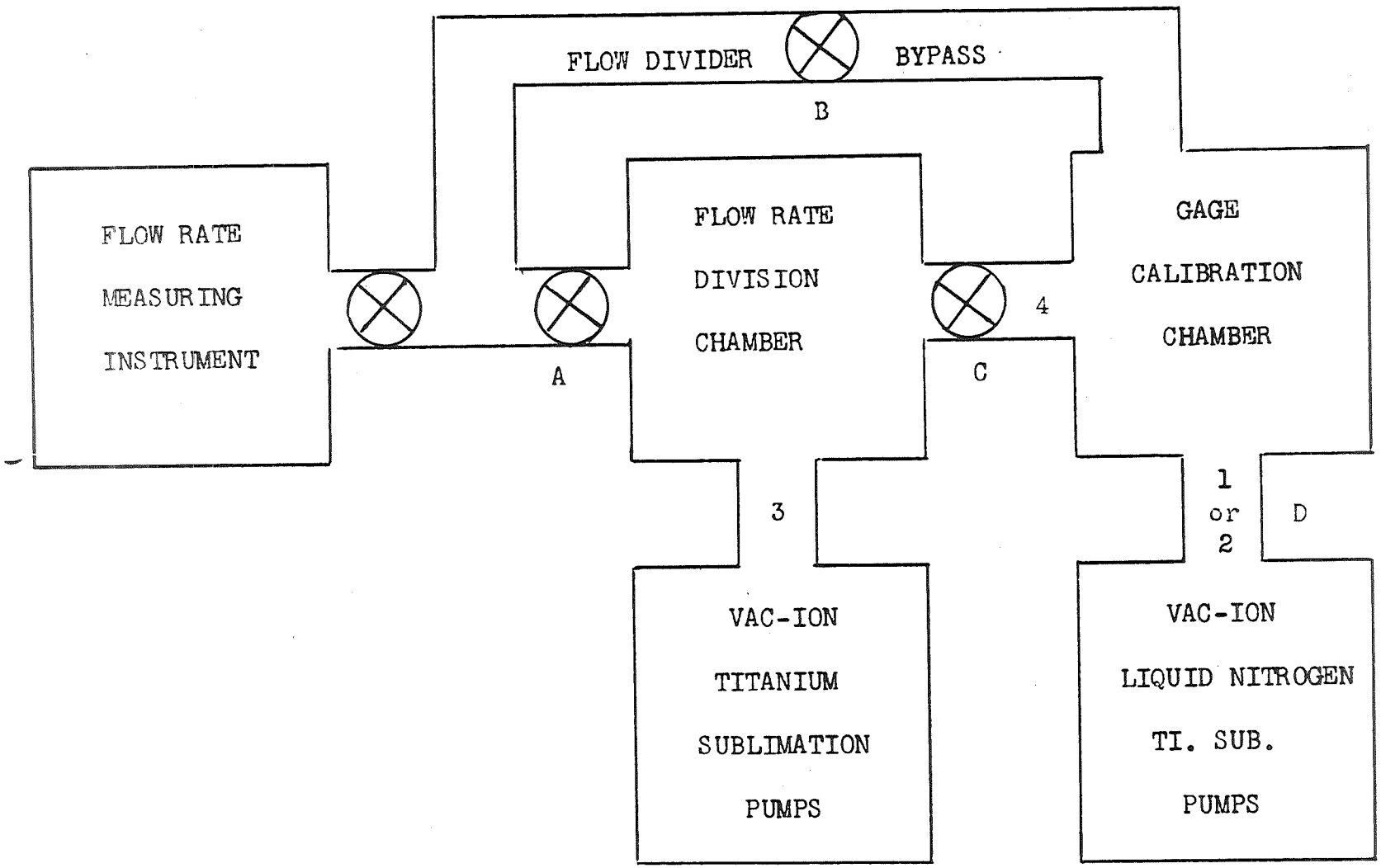


Figure 29.-Block diagram of vacuum gage calibration system.

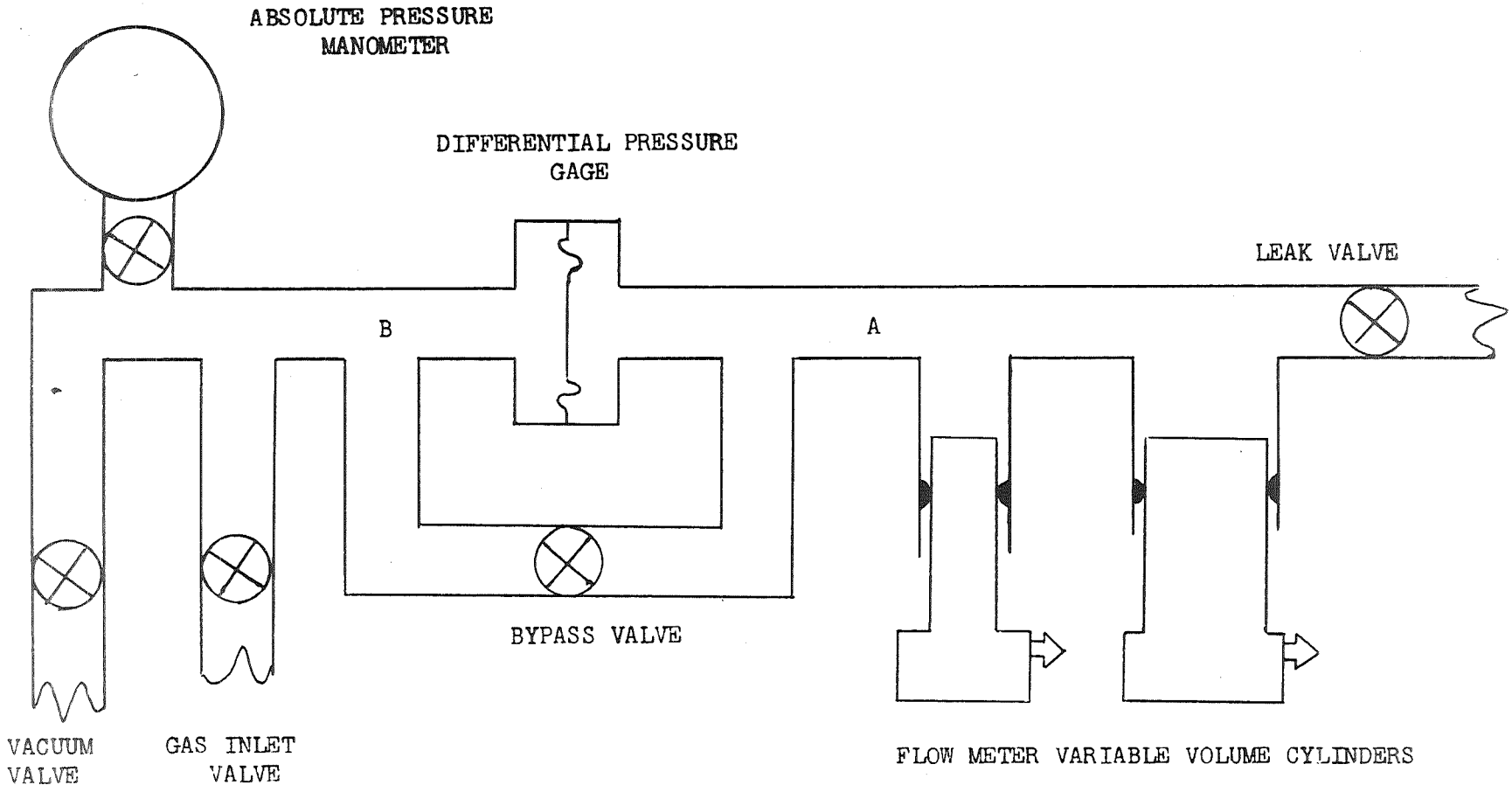


Figure 30.-Block diagram of gas flow rate manometer used with gage calibration system.

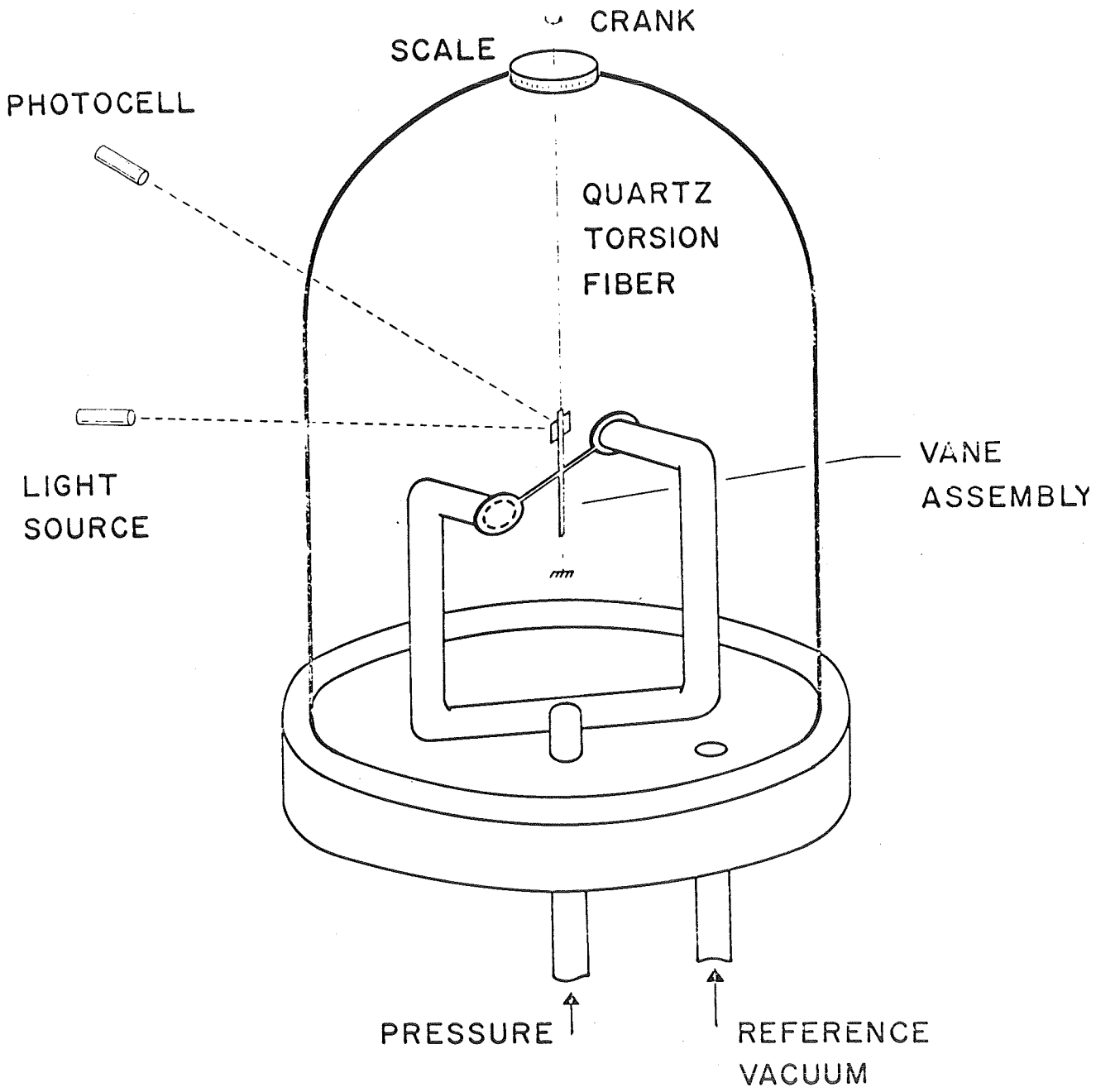


Figure 31.-Schematic drawing of quartz vane gage.

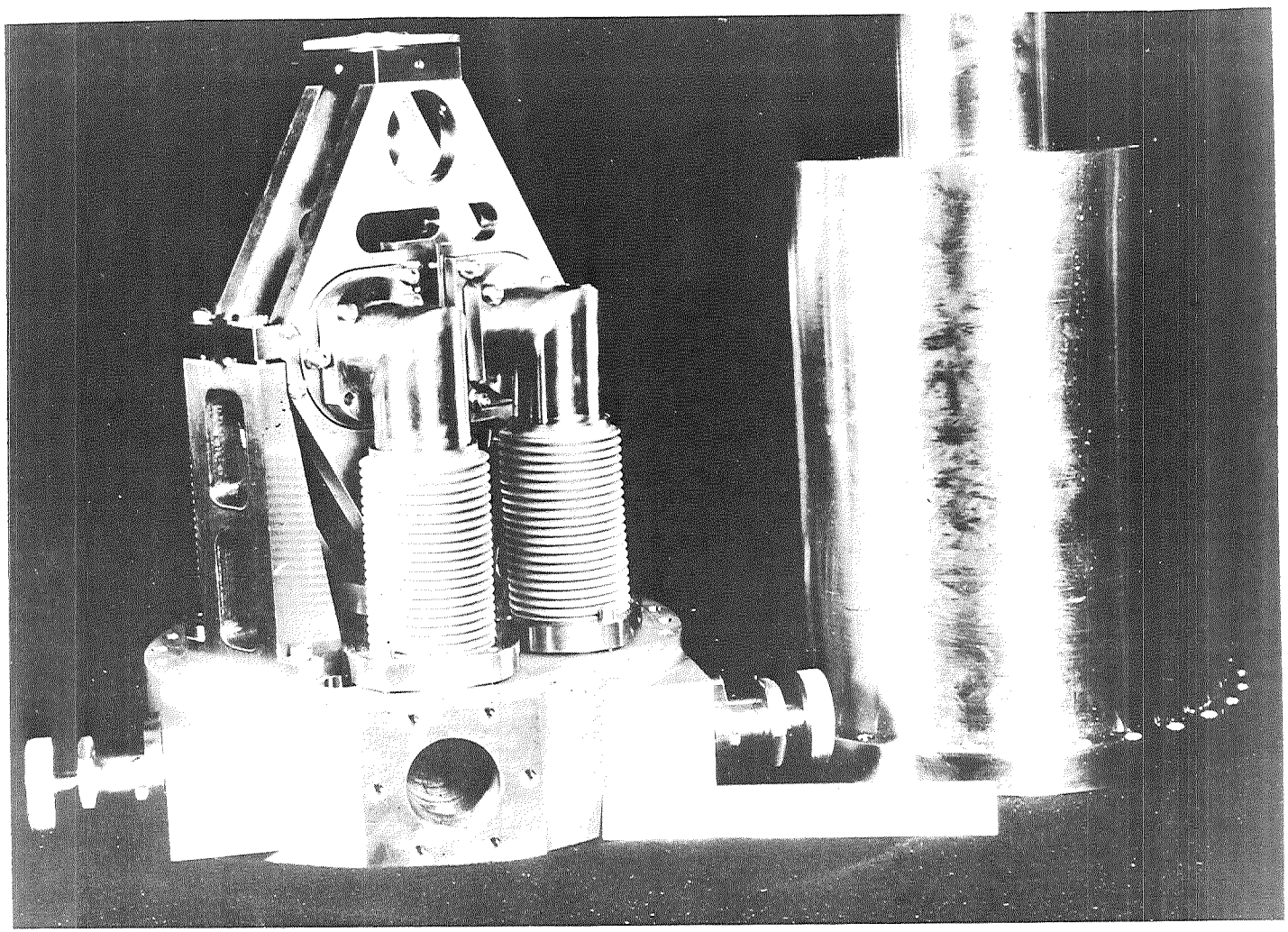

Figure 32.-National Bureau of Standards developmental vane gage.

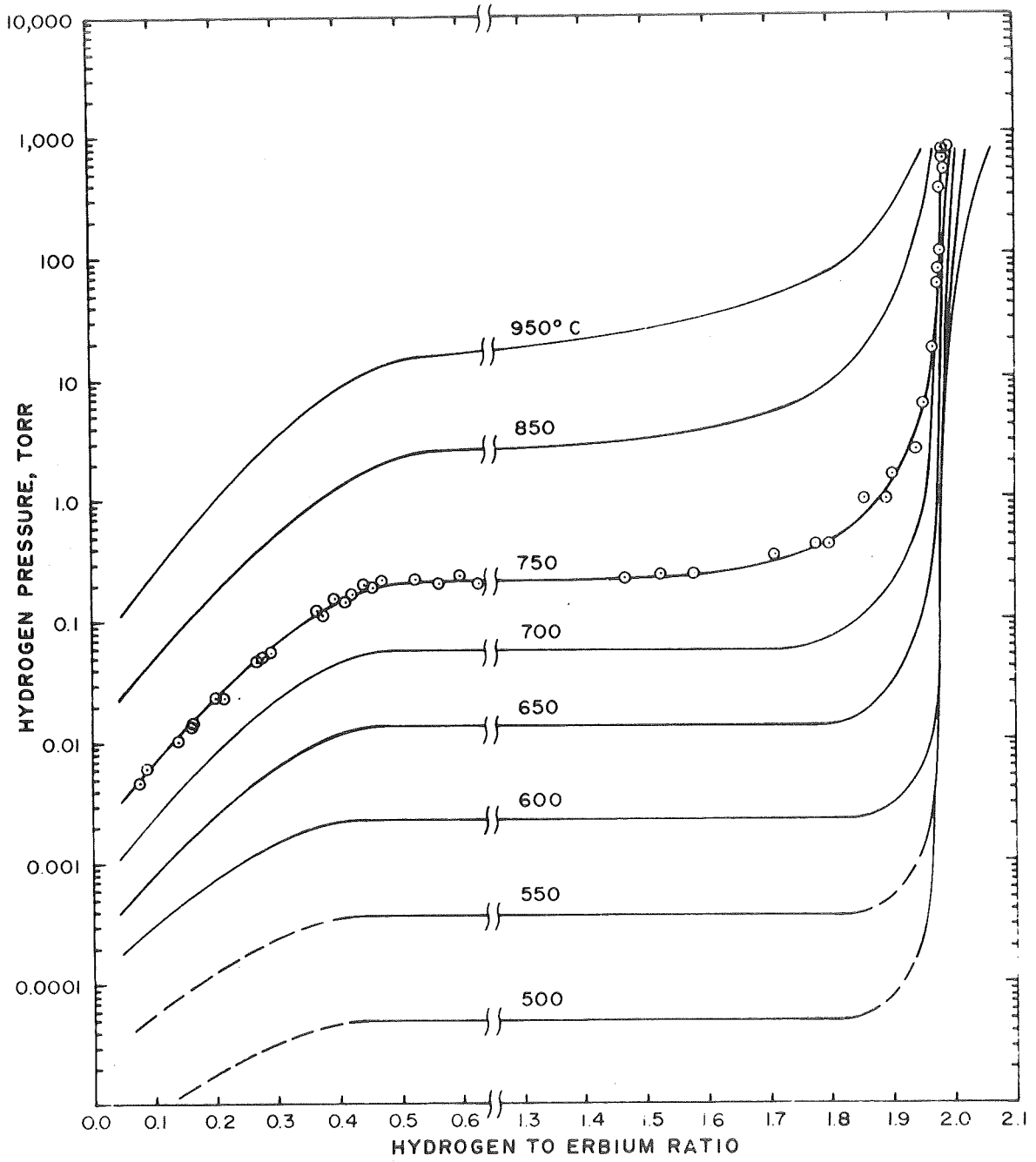


Figure 33.-Family of isotherms in the Erbium-Hydrogen systems.

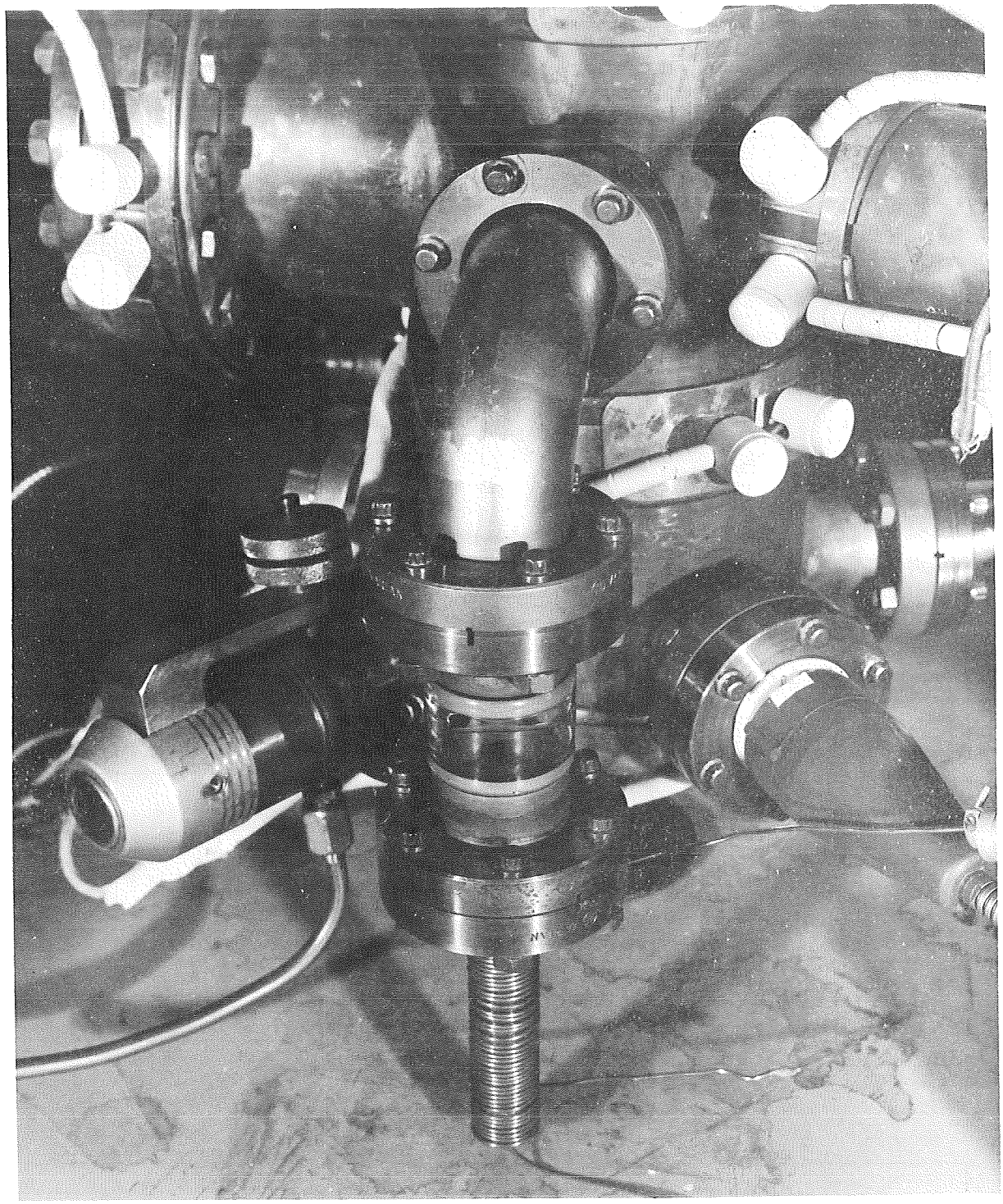

Figure 34.-Hydrogen-Erbium experimental apparatus mounted on vacuum system.

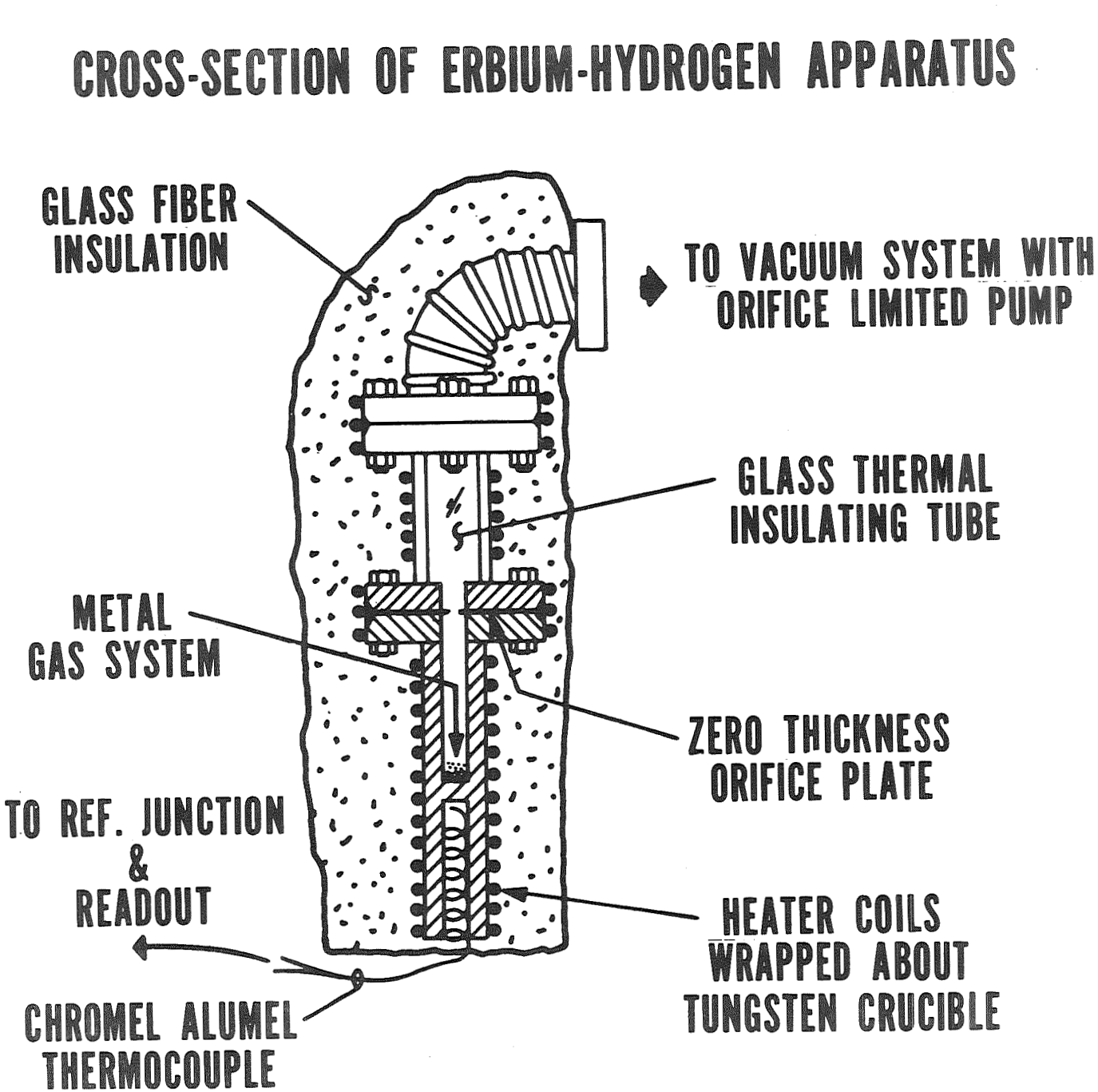


Figure 35.-Schematic drawing of Hydrogen-Erbium experimental apparatus.